Biomedicine & Pharmacotherapy 178 (2024) 117206

Contents lists available at ScienceDirect

Biomedicine & Pharmacotherapy

journal homepage: www.elsevier.com/locate/biopha

Interference with mitochondrial function as part of the antifibrogenic effect of Rilpivirine: A step towards novel targets in hepatic stellate cell activation

Ana M. Benedicto [a,b], Federico Lucantoni [c], Isabel Fuster-Martínez [a,b], Pedro Diaz-Pozo [b], Dimitri Dorcaratto [d,e], Elena Muñoz-Forner [d,e], Victor M. Victor [b,e,f,g], Juan V. Esplugues [a,b,g], Ana Blas-García [b,f,g,1], Nadezda Apostolova [a,b,g,*,1]

[a] Departamento de Farmacología, Facultad de Medicina, Universidad de Valencia, Valencia, Spain
[b] FISABIO–Hospital Universitario Dr. Peset, Valencia, Spain
[c] Laboratory of Cellular Stress and Cell Death Pathways, Centro de Investigación Príncipe Felipe (CIPF), Valencia, Spain
[d] Unidad de Cirugía Hepato-Bilio-Pancreática, Hospital Clínico Universitario, Valencia, Spain
[e] INCLIVA (Instituto de Investigación Sanitaria), Valencia, Spain
[f] Departamento de Fisiología, Facultad de Medicina, Universidad de Valencia, Valencia, Spain
[g] CIBERehd (Centro de Investigación Biomédica en Red de Enfermedades Hepáticas y Digestivas), Valencia, Spain

ARTICLE INFO

Keywords:
Liver fibrosis
Hepatic stellate cells
Therapeutic targets
Mitochondria
Rilpivirine
TGF-β

ABSTRACT

Activated hepatic stellate cells (aHSCs), the main perpetrators of liver fibrosis, are a promising therapeutic target in the treatment of chronic liver disease. During liver injury, HSCs transcend from a quiescent to a fibrotic phenotype, a process which involves major metabolic reprogramming with altered mitochondrial function. The antiretroviral drug Rilpivirine (RPV) has demonstrated a hepatoprotective and specifically antifibrotic effect in several animal models of chronic liver injury, as well as *in vitro*. Herein, we use HSCs activated with the pro-fibrogenic cytokine TGF-β to explore whether mitochondrial function is implicated in this effect. The mitochondrial bioenergetic profile, morphology and dynamics of TGF-β-treated cells (48 h) were altered and these effects were prevented by co-treatment with clinically relevant concentrations of RPV. A MitoStress Test (Seahorse Analyzer) revealed that TGF-β increased both oxygen consumption rate (basal respiration, maximal respiration and spare respiratory capacity) and extracellular acidification rate (indicative of increased glycolysis). Cells exposed to TGF-β also displayed diminished mitochondrial membrane potential and enhanced mitochondrial fission. All of these effects were rescued with RPV. RNA sequencing analysis of cells exposed to TGF-β revealed the presence of 338 differentially expressed genes that encode mitochondrial proteins (mitoDEGs), of which 139 and 199 were significantly up- and down-regulated (adjusted $p<0.05$). This alteration in 15 (10.79 %) and 31 (22.03 %) of the up-regulated and 16 (8.04 %) and 49 (24.62 %) of the down-regulated mitoDEGs was prevented with co-exposure to RPV 4μM or 8μM, respectively. In conclusion, alterations in mitochondrial function are implicated in the antifibrogenic action of RPV, pointing to potential novel antifibrotic targets.

1. Introduction

Liver fibrosis (LF) is a reversible wound-healing response that operates as a common pathophysiologic process converging in various chronic hepatic diseases (CLDs), such as alcoholic liver disease, viral infection and metabolic dysfunction-associated steatotic liver disease (MASLD) (previously known as non-alcoholic fatty liver disease, NAFLD) [1]. Advanced LF is strongly associated with cirrhosis, portal

Abbreviations: DEGs, differentially expressed genes; ECAR, extracellular acidification rate; IMM, inner mitochondrial membrane; HSCs, hepatic stellate cells; aHSCs, activated hepatic stellate cells; CLD, chronic liver diseases; LF, liver fibrosis; MASLD, metabolic dysfunction-associated steatotic liver disease; OCR, oxygen consumption rate; OMM, outer mitochondrial membrane; OXPHOS, oxidative phosphorylation; RPV, rilpivirine; ROS, reactive oxygen species; TGF-β, transforming growth factor beta.

* Correspondence to: Avda Blasco Ibañez n.15-17, Valencia 46010, Spain.
E-mail address: nadezda.apostolova@uv.es (N. Apostolova).
[1] These authors have contributed equally

https://doi.org/10.1016/j.biopha.2024.117206
Received 15 February 2024; Received in revised form 15 July 2024; Accepted 23 July 2024
Available online 29 July 2024
0753-3322/© 2024 The Authors. Published by Elsevier Masson SAS. This is an open access article under the CC BY-NC-ND license (http://creativecommons.org/licenses/by-nc-nd/4.0/).

hypertension, development of hepatocellular carcinoma and end-stage liver failure [2]. The main cell type underpinning LF are hepatic stellate cells (HSCs), which during the process of liver injury, transform from quiescent and lipid-storing to cells with proliferative, contractile, migratory and fibrotic phenotype (activated, aHSCs) characterized by excessive accumulation of an extracellular matrix containing collagen I and III, among other proteins [3,4]. This process is induced by inflammatory mediators of different cellular sources, reactive oxygen species (ROS) and apoptotic bodies mainly arising from dying hepatocytes. It is also stimulated by several profibrogenic cytokines and growth factors, such as transforming growth factor beta (TGF-β), which is pivotal and has been investigated as a target for therapy. It activates HSCs *in vivo*, and a dramatic reduction in alpha smooth muscle actin (α-SMA)-positive cells with a consecutive decrease in collagen deposition has been reported in a TGF-β KO model with LF [5]. Abundant evidence suggests that reversing aHSCs to the quiescent phenotype or inducing their apoptosis alleviates LF. Thus, targeting the activation of HSCs is undoubtedly a promising therapeutic strategy for treating LF [6].

Mitochondrial and metabolic homeostasis are particularly affected during HSC activation, and there is evidence that aHSCs are highly energetic cells, exhibiting increased activity of both glycolysis and mitochondrial respiration [7,8]. Related to this idea, it has been shown that mild mitochondrial uncoupling can inhibit HSC activation *in vitro* [9,10]. Similarly, multiple pharmacological treatments (doxorubicin, astaxanthin and saikosaponin) seem to inhibit HSC activation by suppressing oxidative phosphorylation (OXPHOS) and undermining mitochondrial function [11–13]. Mitochondria also participate in HSC activation through enhanced generation of ROS, and this action includes several mechanisms, such as glutathione depletion and activation of transcription factors [14]. Indeed, collagen type I promoter can be regulated by ROS generation in HSCs, thereby pointing to a fundamental role for oxidative stress in liver fibrosis perpetuation [15]. Mitochondria are highly dynamic organelles in constant balance between fission and fusion, and these shifts regulate their morphology and function. While it is clear that altered mitochondrial dynamics is part of most, if not all, CLDs, the vast majority of studies refer to hepatocytes and how mitochondrial dynamics participate in the activation of HSCs and liver fibrogenesis is poorly understood.

It is also relevant that the antifibrotic actions of certain drugs shown to be protective in the context of HSC activation include effects on mitochondria. Such is the case of the dipeptidyl peptidase-4 inhibitor gemigliptin, an orally administered antidiabetic drug, which was seen to alleviate succinate-induced HSC activation by ameliorating mitochondrial dysfunction, including mitochondrial fission and ROS production, both *in vitro* in LX2 cells and in a mouse model of metabolic dysfunction-associated steatohepatitis (MASH) [16].

Furthermore, apart from the intense search for novel antifibrotic drugs, the repositioning of already existing medicines approved for other indications, is an attractive prospect for the field of liver pathology therapeutics. We have reported that rilpivirine (RPV), an antiretroviral drug widely employed in the treatment of HIV infection, is hepatoprotective and ameliorates LF in different animal models of chronic liver injury [17]. RPV impairs TGF-β-activation of cultured HSCs, as demonstrated by its negative effect on the levels of general profibrotic markers such as alpha-1 type I collagen (COL1A1), α-SMA, platelet-derived growth factor B (PDGFB), vimentin, plasminogen activator inhibitor-1 (*SERPINE1*/PAI-1) and TGF-β, and signal transducer and activator of transcription 3 (pSTAT3), a transcription factor crucial for HSC proliferation and activation. In addition, RPV stimulates autophagic flux in aHSCs, an effect associated with its capacity to undermine the cells' viability at high concentrations (8μM RPV) [18].

With the aim of better understanding the antifibrotic effect of RPV and identification of novel therapeutic targets for LF, the present *in vitro* study was designed to investigate the capacity of RPV to interfere with mitochondrial function during HSC activation.

2. Material and methods

2.1. Reagents

Unless stated otherwise, chemicals were from Sigma-Aldrich. RPV (Sequoia Research Products) was dissolved in DMSO (stock 5 mM, employed at a final concentration of 1–8 μM), a solvent used as a control treatment (denoted as "vehicle") and employed for all statistical comparisons. TGF-β1 (Myltenyi Biotec) was also dissolved in DMSO (stock 10 μg/mL, employed at 2.5 ng/mL).

2.2. Cell culture and treatment

LX2 cells are an immortalized human HSC line which has been extensively characterized and retains key features of signaling and metabolism, making it a suitable model of human hepatic fibrogenesis [19]. It was purchased from Sigma-Aldrich and routinely cultured in DMEM with a high glucose concentration supplemented with 10 % iFBS, 50 U/mL penicillin and 50 μg/mL streptomycin. Subculturing was performed using 0.25 % Trypsin-EDTA and subconfluent cell cultures of passage number lower than 25 were used for all the experiments.

Human primary HSC were isolated from macroscopically healthy liver specimens taken from freshly resected liver tissue of patients during surgical interventions due to primary or secondary liver tumors (gender: 4 male and 2 female, ages: 51–80, mean age: 65.7 years). Informed consent was obtained from patients for the use of tissue for research purposes according to the ethical guidelines of *Hospital Universitario Clínico*, Valencia, Spain (ref. 2018/272). Cell isolation was performed according to the protocol described by Casini et al. [20]. After washing with Hanks' balanced salt solution (HBSS) at 37ºC, liver samples were carefully minced with a sterile razor blade inside a sterile flask containing 0.5 % pronase (Sigma-Aldrich), 0.05 % type IV collagenase (Sigma-Aldrich), 5 μg/mL of deoxyribonuclease I (DNase I) (Sigma-Aldrich) in 100 mL of HBSS without Ca^{2+}/Mg^{2+}, and shaken (30 min, 37ºC). The obtained cell suspension was filtered through two metal strainers placed one above the other, and the filtration process was repeated using a Falcon® 100 μm cell strainer. The filtered solution was washed several times in HBSS and centrifuged (5 min, 500 g). The obtained cell pellet was resuspended in 25 mL of the same solution. To separate HSCs from the rest of the cells and debris, a three-step Percoll (GE Healthcare Life Sciences) gradient centrifugation (100 %, 50 % and 35 % v/v) was performed (274 g, 30 min, 4ºC). HSCs were located in the interphase between the medium and the 35 % gradient. To initially culture HSCs, they were plated onto cell culture flasks in DMEM medium with a high glucose concentration, 20 % FBS, 50 U/mL penicillin, 50 μg/mL streptomycin and 0.25 μg/mL amphotericin B. The medium was changed 24 h after initial plating and at 72 h from thereafter.

Cell cultures were maintained in a cell culture incubator (MCO-19AICUV-PE, Panasonic Healthcare Co. Ltd.) at 37ºC, with a humidified 5 % CO_2/95 % air atmosphere (AirLiquide Medical). Cells were activated with the profibrotic cytokine TGF-β for 48 h and co-treated with clinically relevant concentrations of RPV or with vehicle.

2.3. Western blotting

SDS-PAGE and protein transfer to nitrocellulose membranes were performed using standard techniques (Bio-Rad Laboratories). In order to isolate the whole-cell proteins, liver samples (20–35 mg) were homogenized in 900 μL extraction buffer (0.066 M Tris-HCl pH 7.5, 1 mM EGTA, 1 mM Na_3VO_4, 1 μM NaF and the protease inhibitor Complete Mini™ Protease Inhibitor Cocktail from Merck) using a MACS™ Dissociator (MACS Miltenyi Biotec). After adding 10 μL of 10 % NP-40 Surfact-Amps™ (ThermoFisher Scientific), samples were sonicated (5 min, 15ºC) and centrifuged (16000 g, 40 min, 4ºC). For cell culture, cell pellets were lysed in 75–100 μL of PhosphoSafe™Extraction Reagent (EMD Millipore Corp.) supplemented with Complete Mini™ Protease

Inhibitor Cocktail, and vortexed (15 sec), incubated (5 min) and centrifuged (4°C, 5 min, 16000 rpm). In both cases, protein content was quantified by the BCA assay (Pierce™ BCA Protein Assay Kit, ThermoFisher Scientific). Primary antibodies included rabbit polyclonal anti-MT-ND1 (Abcam, ref. ab74257), anti-porin (Abcam, ref. ab14734), anti-GRP75 (Abcam, ref. ab53098), anti-DRP1 (Cell Signaling Technology, ref. 8570 S), anti-p-DRP1 (Cell Signaling Technology, ref. 3544 S), rabbit polyclonal anti-GAPDH (Sigma-Aldrich, ref. G9545, 1:20,000), mouse polyclonal anti-mitofusin 2 (Abcam, ref. ab56889) and mouse monoclonal anti-OPA1 (BD Biosciences, ref. 612606), all used at 1:1000 dilution. The secondary antibodies were anti-rabbit (1:5.000, Vector laboratories, ref. PI-1000) and anti-mouse (1:2000, Invitrogen, ref. 32230). Immunolabeling was detected by enhanced chemiluminescence visualized with a digital luminescent image analyser (ImageQuant 800, Amersham), employing Luminata™ Crescendo Western HRP substrate (Merck), or SuperSignal™ West Femto Maximum Sensitivity Substrate (ThermoFisher Scientific). Protein expression is represented as a percentage of control (average expression in the control group was considered 100 %), using GAPDH (glyceraldehyde 3-phosphate dehydrogenase) as a loading control. Densitometric analysis was performed using ImageJ software (Fiji).

2.4. Fluorescence microscopy

In all cases, cells were seeded (1.5×10^4 /well) in a sterile μ-Slide 8 well chamber slide (Ibidi) and treated for 48 h. Imaging was performed at the Central Unit for Research in Medicine, University of Valencia, Valencia, Spain, with the Leica TCS-SP8 confocal laser scanning unit (Leica Microsystems), with a 405 diode and white light lasers attached to a Leica DMi8 inverted microscope with a heated and CO_2-incubated stage. Images were captured at 63× (HC PL APO 63.0×/1.40 oil CS2) or 40× magnification (HC PL APO 40×/1.30 Oil CS2) objective.

2.4.1. Mitochondrial mass and morphology

Live cell staining of mitochondria was performed with dyes that do not depend on mitochondrial membrane potential. After treatment, cells were incubated with 100 nM NAO (10-nonyl acridine orange, ThermoFisher), a green-fluorescent compound that specifically binds to cardiolipin, an inner mitochondrial membrane (IMM) phospholipid, or 100 nM MitoView 650 (Biotium), a far-red mitochondrial stain suitable for no-wash, long-term staining in live cells, and 100 nM Hoechst 33342 (Sigma-Aldrich) to stain nuclei for 30 min at 37°C. Subsequently, the medium was removed, cells were washed with Krebs Buffer (KB) and incubated with KB containing 5 mM D-glucose, 2.5 mM $CaCl_2$ and 100 nM Hoechst 33342 during imaging of live cells. For single-cell morphology analysis (Mitoview fluorescence), deconvolved stack images were processed with Fiji (ImageJ 1.53f51). In short, the subtract background function was applied with the slightly paraboloid option set to 50 pixels (rolling ball radius). Subsequently, the *MiNA analyze morphology plugin* [21] was employed to obtain the median branch length from each image using an unsharp mask set to 4 radius (sigma) and the max entropy thresholding operation. For image analysis of the mitochondrial mass, we used ImageJ to detect the number of cells and the area and intensity of the NAO staining. The parameters used to evaluate the mitochondrial mass were "area stained per cell" and "intensity of the staining per cell".

2.4.2. Mitochondrial membrane potential

Treated cells were stained with 60 nM of tetramethylrhodamine methyl ester (TMRM, Thermofisher) - a cationic, red-orange, fluorescent dye that is readily sequestered by active mitochondria and employed to assess mitochondrial membrane potential ($\Delta\psi_m$) - and with 100 nM Hoechst 33342 – used to stain nuclei - in full medium for 30 min. The cells were subsequently transferred to the microscope without washing. The mitochondrial uncoupler CCCP (Sigma-Aldrich) was added at 50 μM for 30 min before staining as a control treatment. Images were analysed using the CellProfiler 4.2.1. In brief, a "correct illumination" module with a block size of 60 and no smoothing was employed to reduce the background signal. A "smooth" module was then applied to enlarge the fluorescence signal and the image obtained was processed with an "identify secondary objects" module to obtain pseudo-cytoplasm objects. An "identify primary objects" module was employed to extrapolate mitochondrial object from the TMRM signal and related to the cytoplasm. Finally, a "measure object intensity" module was applied to obtain the mean intensity of each mitochondrial object.

2.4.3. Mitochondrial superoxide production

Treated cells were stained with 1 μM MitoSox (ThermoFisher), a cationic derivative of dihydroethidum (DHE) designed to detect mitochondrial superoxide in living cells, and with 100 nM Hoechst 33342, used to stain nuclei, in HBSS for 30 min. Subsequently, they were washed with HBSS and transferred immediately to the microscope. The positive control was the inhibitor of complex I at the mitochondrial electron transport chain rotenone (25 μM), which was added 1 h before staining. The image analysis of the MitoSox signal was performed by ImageJ in order to detect the number of cells, and the area and intensity of the fluorescence. The parameters used for the evaluation of the mitochondrial mass were "area stained per cell" and "intensity of the staining per cell".

2.5. Transmission electron microscopy

Transmission electron microscopy (TEM) was performed at the core electron microscopy facility of the Principe Felipe Research Center (CIPF), Valencia, Spain. Cells were seeded (1×10^4/well) in sterile 8-well chamber slide plates (Nunc) and treated for 48 h. They were then fixed in 3 % glutaraldehyde in 0.1 M phosphate buffer (PB) for 10 min at 37ºC, washed in PB and fixed again in glutaraldehyde for 2 h at room temperature. Next, they were washed in 0.1 M PB, 5 times over a 10-min period and stored at 4 ºC. The samples were postfixed in 2 % OsO_4 for 1 h at room temperature and stained in 2 % uranyl acetate in the dark for 2 h at 4°C. Afterwards, they were rinsed in distilled water, dehydrated in ethanol and infiltrated overnight in Durcupan resin (Sigma-Aldrich). Following polymerization, embedded cultures were detached from the wells and glued to Durcupan blocks. Finally, ultra-thin sections (0.08 μm) were cut with an Ultracut UC-6 (Leica microsystem), stained with lead citrate (Reynolds solution) and examined under a transmission electron microscope FEI Tecnai Spirit BioTwin (ThermoFisher Scientific company). Photomicrographs were taken with a Xarosa digital camera (EMSIS GmbH) controlled by Radius software (Version 2.1).

Mitochondrial size and shape were measured using Fiji (ImageJ 1.53f51) by manually tracing mitochondria with clearly discernible outlines on TEM micrographs [22]. Surface area (mitochondrial size) is reported in square micrometers; perimeter in micrometers; aspect ratio is computed as [(major axis)/(minor axis)] and reflects the "length--to-width ratio"; form factor [(perimeter^2)/(4π·surface area)] reflects the complexity and branching aspect of mitochondria; circularity [4π·(surface area/perimeter^2)] and roundness [4·(surface area)/(π·major axis^2)] are two-dimensional indexes of sphericity with values of 1 indicating perfect spheroids; for example, circularity signifies the comparability of the shape to a circle, and it is the ratio between the actual area and the area of a circle of the same length, so this factor increases as the shape of the mitochondrion becomes more circular.

2.6. Analysis of bioenergetics by Seahorse XF analyzer

These experiments were performed at FISABIO–Hospital Universitario Dr. Peset, Valencia, Spain. Seahorse XF Analyzer (Agilent) is a widely recognized, standard technology employed to assess the bioenergetic state of live cells, as it simultaneously measures in real-time the oxygen consumption rate (OCR) and extracellular acidification rate (ECAR), indicative of glycolysis. Cells were seeded (1×10^4/well, in

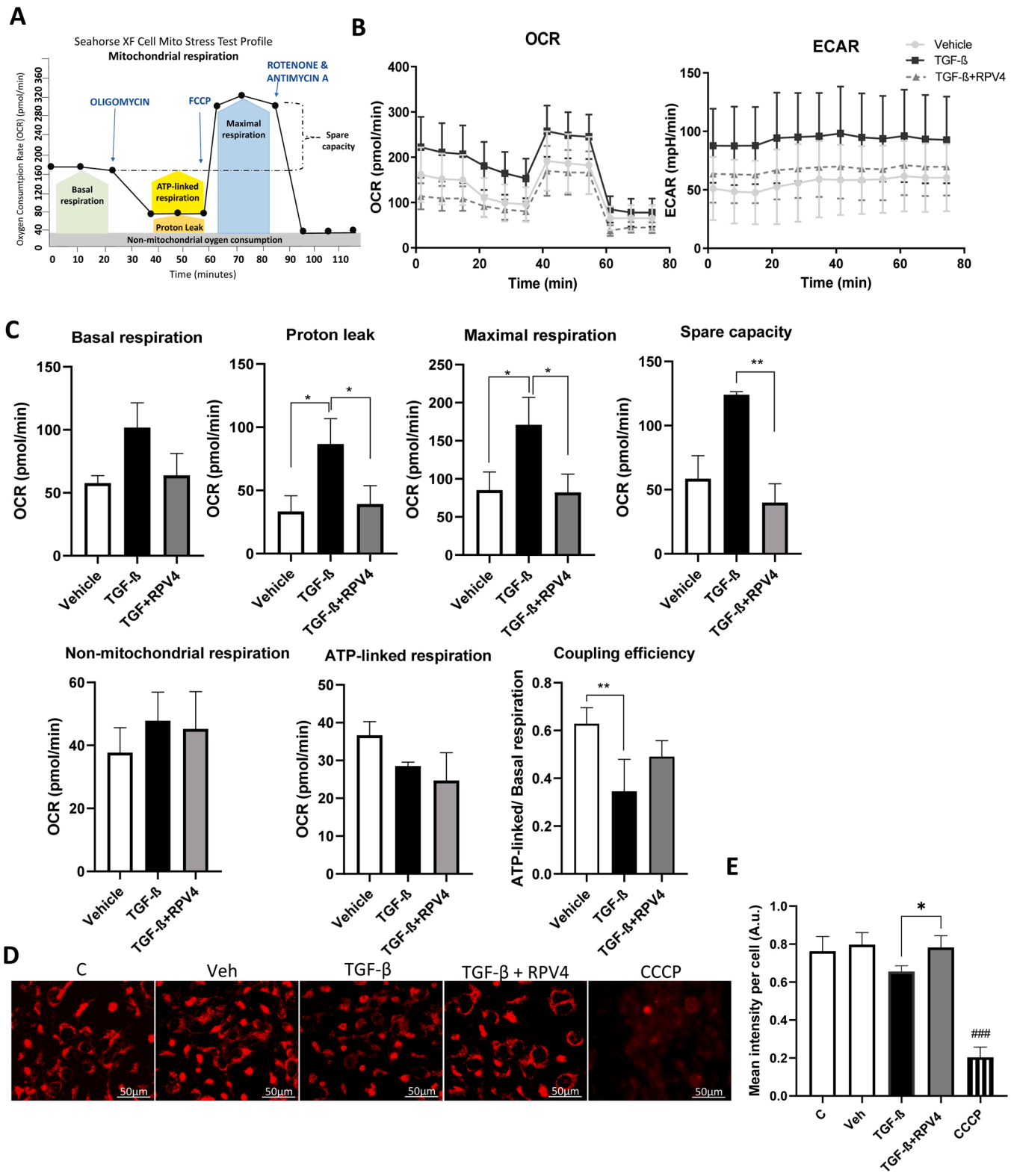

Fig. 1. Analysis of mitochondrial function. LX2 cells were treated for 48 h with Vehicle (Veh), TGF-β alone or TGF-β in the presence of 4 μM RPV. (A) Schematic representation of the Seahorse MitoStress bioenergetic test workflow and parameters that are determined. (B) Oxygen consumption rate (OCR) and Extracellular acidification rate (ECAR) data. (C) Quantification of several standard parameters in the Seahorse analysis. Data were normalized to the total amount of protein per sample, represented as mean±SEM (n=3, except for TGF-β in "Spare capacity" where n=2) and analyzed by one-tailed paired Student́s t-test of TGF-β vs Veh or TGF-β+RPV4 vs TGF-β (* and ** represent a p value <0.05 or <0.01, respectively). (D) Mitochondrial membrane potential ($\Delta\Psi_m$) was studied by live cell fluorescence microscopy and the mitochondrial uncoupler CCCP (30 μM, 30 min) was employed as a control condition for loss of $\Delta\Psi_m$. Representative images (20x) of cells stained with tetramethyl rhodamine (60 nM TMRM), used to assess $\Delta\Psi_m$ (red signal) are shown. (E) Quantification of the fluorescence data was performed by Cell Profiler and data (mean±SEM, n=3) were analyzed by Student́s t-test of TGF-β+RPV4 vs TGF-β (* represents a p value <0.05) or of CCCP vs Veh (### represents a p value <0.001).

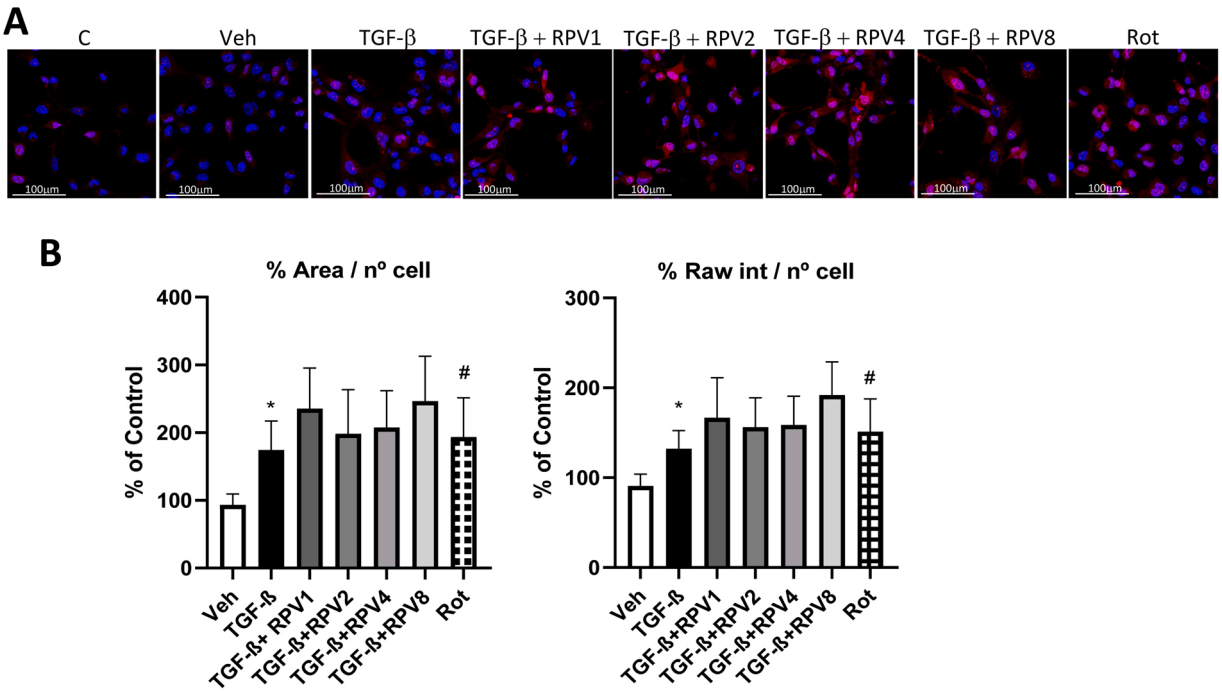

Fig. 2. Analysis of mitochondrial superoxide content. LX2 cells were treated for 48 h with Vehicle (Veh), TGF-β alone or TGF-β in the presence of increasing concentrations of RPV. Treatment with the mitochondrial complex I inhibitor rotenone (Rot) was employed as a positive control condition (25 µM, 1 h-treatment). (A) Representative live cell confocal microscopy images (magnification: 40x) of cells stained with MitoSox (5 µM, to detect mitochondrial superoxide, red fluorescence) and Hoechst 33342 (100 nM, to mark nuclei, blue signal). (B) Quantification of the fluorescence data was performed by ImageJ and data are shown as mean ±SEM, n=6. The fluorescent signal in untreated cells (Control) was considered 100 %. Data were analyzed by a Student's t-test of TGF-β vs Veh (* represents a p value <0.05) or Rot vs Veh (# represents a p value <0.05).

a final volume of 80 µL/well) and treated for 48 h. Mitochondrial function was assessed using the XFp Cell Mito Stress Test Kit (Agilent) (Fig. 1A), following the manufacturer's instructions and the 8-well-Seahorse XF analyzer [23]. Compounds were loaded into the cartridge injection ports, rendering final concentrations of 1.5 µM oligomycin, 1 µM FCCP and 1 µM rotenone/antimycin A. Data were normalized to the protein content in each well (all conditions performed in duplicate); for which immediately after the Seahorse measurement, cells were lysed with RIPA buffer supplemented with protease inhibitors (50 µL/well) and protein concentration was determined by the BCA assay (Pierce™ BCA Protein Assay Kit, ThermoFisher Scientific).

2.7. RNA sequencing

2.7.1. RNA extraction, mRNA libraries and RNA sequencing

This analysis was performed on primary human HSCs treated for 48 h with Vehicle, TGF-β, or TGF-β in the presence of RPV 4µM or 8µM. RNA extraction from cell pellets was performed using the illustra®RNAspin Mini RNA Isolation kit (GE Healthcare) according to the manufacturer's instructions. In brief, cell pellets were resuspended in 350 µL lysis buffer and 3.5 µL ß-mercaptoethanol (ß-ME) and homogenized by passage through a 25 G needle. Next, 350 µL of 70 % ethanol were added and the solution was transferred to a column that retained the RNA. The membrane was desalted and DNA was digested by enzymes. To elute RNA the membrane was washed three times in 30 µL RNase-free water. The purity and concentration of the RNA were determined spectrophotometrically (NanoDrop™ ND-1000 spectrophotometer, Thermo Scientific). For RNA sequencing (performed at the Central Unit for Research in Medicine, University of Valencia, Valencia, Spain), mRNA libraries were prepared from total RNA using the TruSeq Stranded mRNA Library Preparation kit from Illumina, following the manufacturer's protocol. In short, purification of mRNA was performed using dT oligos that bind to the polyA tails of mRNA, thus selecting them specifically. Subsequently, these molecules were fragmented and hybridized with hexamers to synthesize the cDNA. The second standard of the cDNA was synthesized with dUTPs to label it and achieve strand specificity. These double-stranded molecules were ligated to indexed adapters and subsequently enriched by PCR. The libraries thus generated were quantified by fluorimetry and their size was verified using the Agilent Bioanalyzer. An equimolar pool of all samples was prepared and sequenced on the NGS NextSeq 550 platform (Illumina) using 75-cycle single read sequencing (1×75 bp).

2.7.2. Transcriptomic analysis

The bioinformatic analysis was performed by the CIBEREHD (*Centro de Investigación Biomédica en Red: Enfermedades Hepáticas y Digestivas*, Spain) Bioinformatics Service. Processing of raw reads including quality control, trimming for Illumina adapters, filtering, alignment to the human genome and gene quantification were performed as previously [24]. We used DESeq [25] on raw counts for identifying differentially expressed genes (DEGs). Volcano plots and plots of principal component analysis (PCA) were obtained using the R statistical software with ggplot2 3.4.4 and ggfortify 0.4.16 packages.

2.8. Statistical analysis and presentation of data

All images are representative of at least 3 independent experiments. In most cases, data are represented as % of control, with untreated cells considered 100 %. Data are shown as mean±SEM and analysed using GraphPad Prism V.8.01 (GraphPad Software) with an unpaired or paired Student's t-test or a one-way analysis of variance (ANOVA) followed by a Dunnett's multiple comparison test. $^{*}p<0.05$ and $^{\#}p<0.05$ were considered statistically significant.

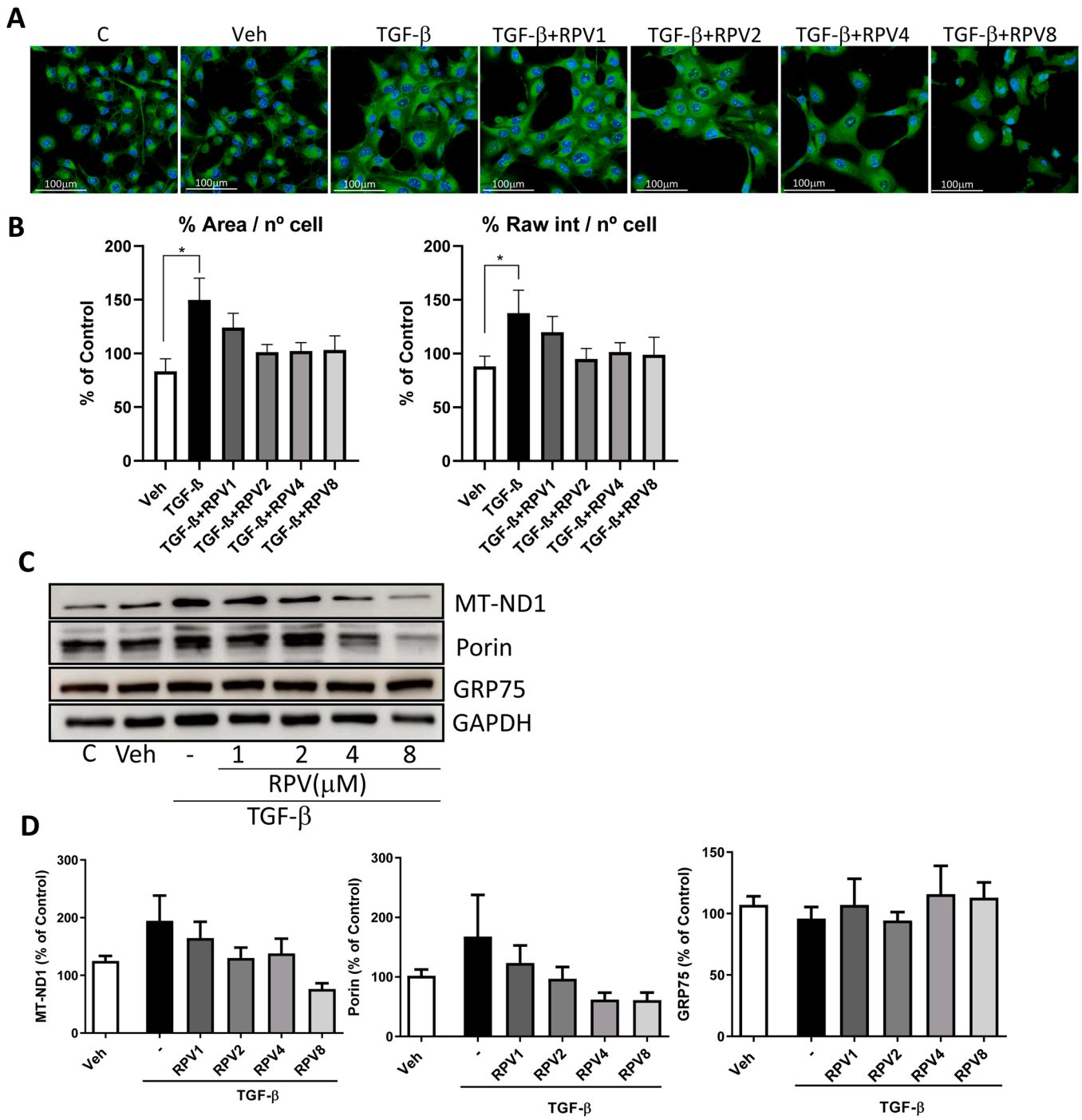

Fig. 3. Analysis of mitochondrial mass. LX2 cells were treated for 48 h with Vehicle (Veh), TGF-β alone or TGF-β in the presence of increasing concentrations of RPV. (A) Representative live cell confocal microscopy images (magnification: 40x) of cells stained with the mitochodnrial dye 10-nonyl-acridine orange (200 nM NAO) green signal and Hoechst 33342 (100 nM, to mark nuclei, blue signal). (B) Quantification of the fluorescence data was performed by ImageJ and data are shown as mean±SEM, n=6. The fluorescent signal in untreated cells (Control) was considered 100 %. Data were analyzed by Student́s t-test of TGF-β vs Veh (* represents a p value <0.05). (C) Analysis of the content of marker proteins by Western Blot in whole-cell protein extracts. Representative images and quantification of data (mean ±SEM, n=4–8) (D) are shown. GAPDH was employed as a loading control and data in untreated cells were considered 100 %.

3. Results

3.1. Effect of rilpivirine on mitochondrial function

Firstly, we addressed the bioenergetic profile of LX2 cells after 48 h-treatment with TGF-β, alone or in the presence of RPV 4 μM, a concentration that produces evident antifibrotic effects but lacks major cytotoxicity. Using the Seahorse flux analyzer, we detected that exposure to TGF-β increased both OCR and ECAR, and this was prevented by co-treatment with RPV 4 μM (Fig. 1B). A detailed analysis of OCR revealed that basal respiration (the energetic demand of cells under basal conditions), maximal respiration (the maximum capacity that the electron respiratory chain can achieve) and spare respiratory capacity (calculated as the difference between maximal and basal respiration) were all enhanced in TGF-β-treated cells (Fig. 1C). Importantly, this effect was absent in the presence of RPV. Basal respiration is composed

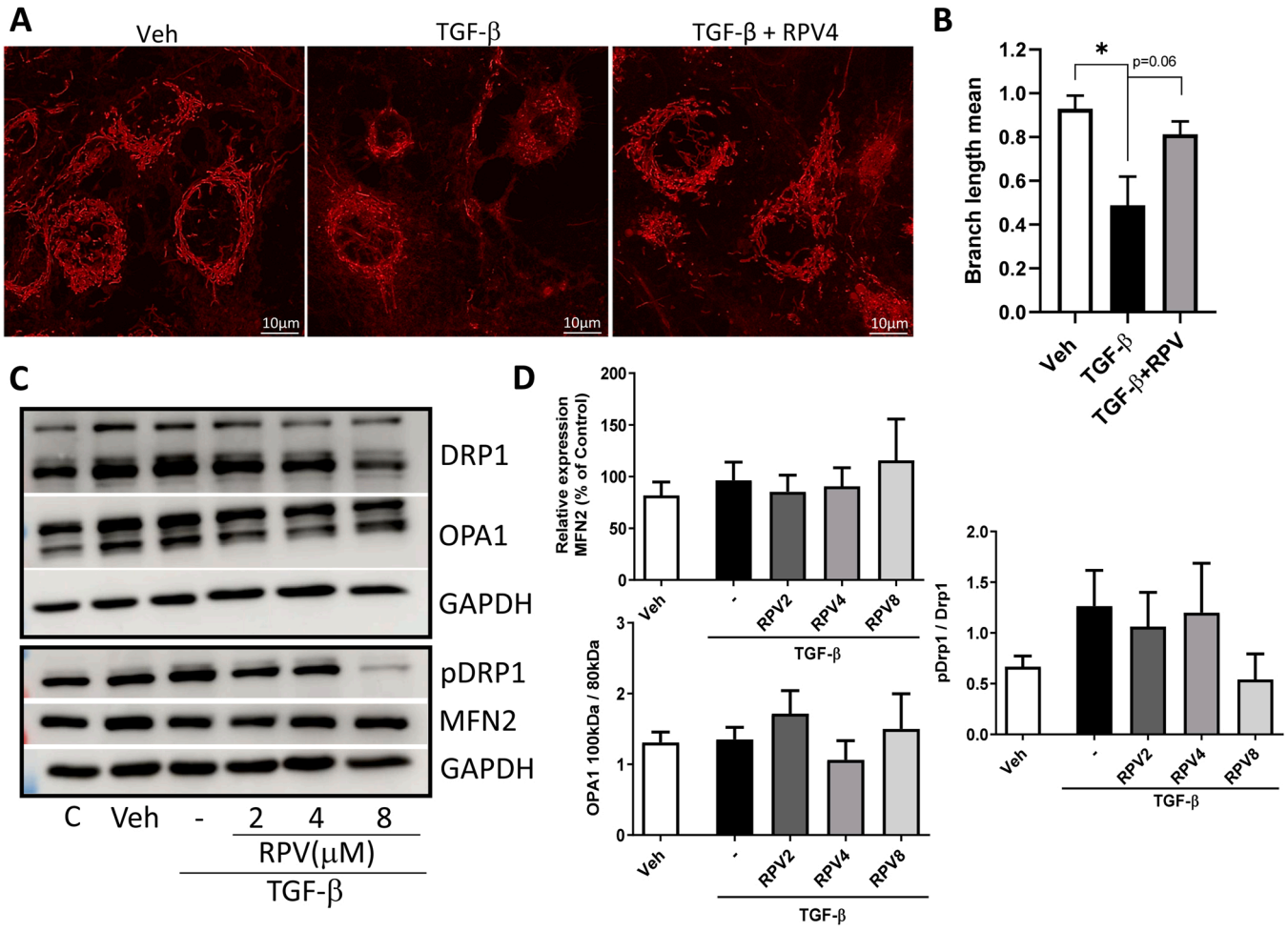

Fig. 4. Analysis of mitochondrial morphology and dynamics. LX2 cells were treated for 48 h with Vehicle (Veh), TGF-β alone or TGF-β in the presence of increasing concentrations of RPV. (A) Representative live cell confocal microscopy images (magnification: 63x) of cells stained with the mitochondrial stain Mitoview 100 nM (red), to study mitochondrial morphology. (B) Fluorescence was quantified by ImageJ and data (mean±SEM, n=4) were analyzed by Student́s t test of TGF-β vs Veh (* represents a *p* value <0.05). (C) Analysis of mitochondrial dynamics (fission and fusion) through assessment of marker proteins (p-DRP-1, OPA-1 and mitofusin 2, MFN2) by Western blot. Representative images and quantification of data (mean±SEM, n=5–7) (D) are shown. GAPDH was employed as a loading control and data from untreated cells were considered 100 % or 1.

of the OCR used to meet ATP synthesis and that resulting in mitochondrial proton leak. Interestingly, we detected that the increase in OCR by TGF-β was due to a rise in proton leak rather than ATP-producing OCR. Finally, non-mitochondrial respiration (the oxygen consumption due to cellular components other than mitochondria) was not affected by TGF-β or RPV. $\Delta\psi_m$ is a fundamental part of mitochondrial function, and so we assessed this parameter through fluorescence microscopy and detected a drop in $\Delta\psi_m$ in LX2 cells exposed to TGF-β for 48 h, an effect that was absent upon co-treatment of TGF-β with RPV (Fig. 1D,E). This result is in line with the data of the Seahorse analysis, which revealed a major increase in proton leak in TGF-β-treated cells that was prevented with RPV.

Finally, we also aimed to study mitochondrial ROS production, for which purpose we assessed mitochondrial superoxide levels through fluorescence microscopy, using the fluorochrome MitoSox and employing 25 μM rotenone as a positive control. Treatment of LX2 cells for 48 h with TGF-β led to an increase in MitoSox fluorescence; however, when assayed in a wide range of 1–8 μM, RPV was not able to prevent it at any of the concentrations employed (Fig. 2).

3.2. *Effect of rilpivirine on mitochondrial mass, morphology and dynamics*

In order to study mitochondrial mass, live cell imaging of LX2 cells was performed using the fluorescent dye NAO. Exposure to TGF-β for 48 h led to an increase in the green signal, both in terms of its area in the cell and its intensity, and this enhancement was lower (RPV 1 μM) or absent (RPV 2, 4 or 8 μM) when co-treated with RPV (Fig. 3A,B). In an additional approach, we evaluated the content of several mitochondrial proteins - MT-ND1 (mitochondrially encoded NADH:ubiquinone oxidoreductase core subunit 1), porin (also termed the voltage-dependent anion channel or VDAC) and GRP75 (glucose-regulated protein 75) – which are markers of the IMM, matrix and outer mitochondrial membrane (OMM), respectively. Exposure to TGF-β did not alter the levels of GRP75, but it significantly increased those of MT-ND1 (a core component of complex I of the mitochondrial electron transport chain) and porin (the most abundant protein in the OMM). Co-exposure to RPV showed a clear tendency to rescue the effect of TGF-β on MT-ND1 and porin; RPV 8 μM led to a major decrease in the presence of these proteins compared to the control (Fig. 3C, D).

The mitochondrial network consists of a complex, branched system of connected mitochondria. In order to assess the effect or TGF-β and TGF-β+RPV on mitochondrial network morphology, cells were stained

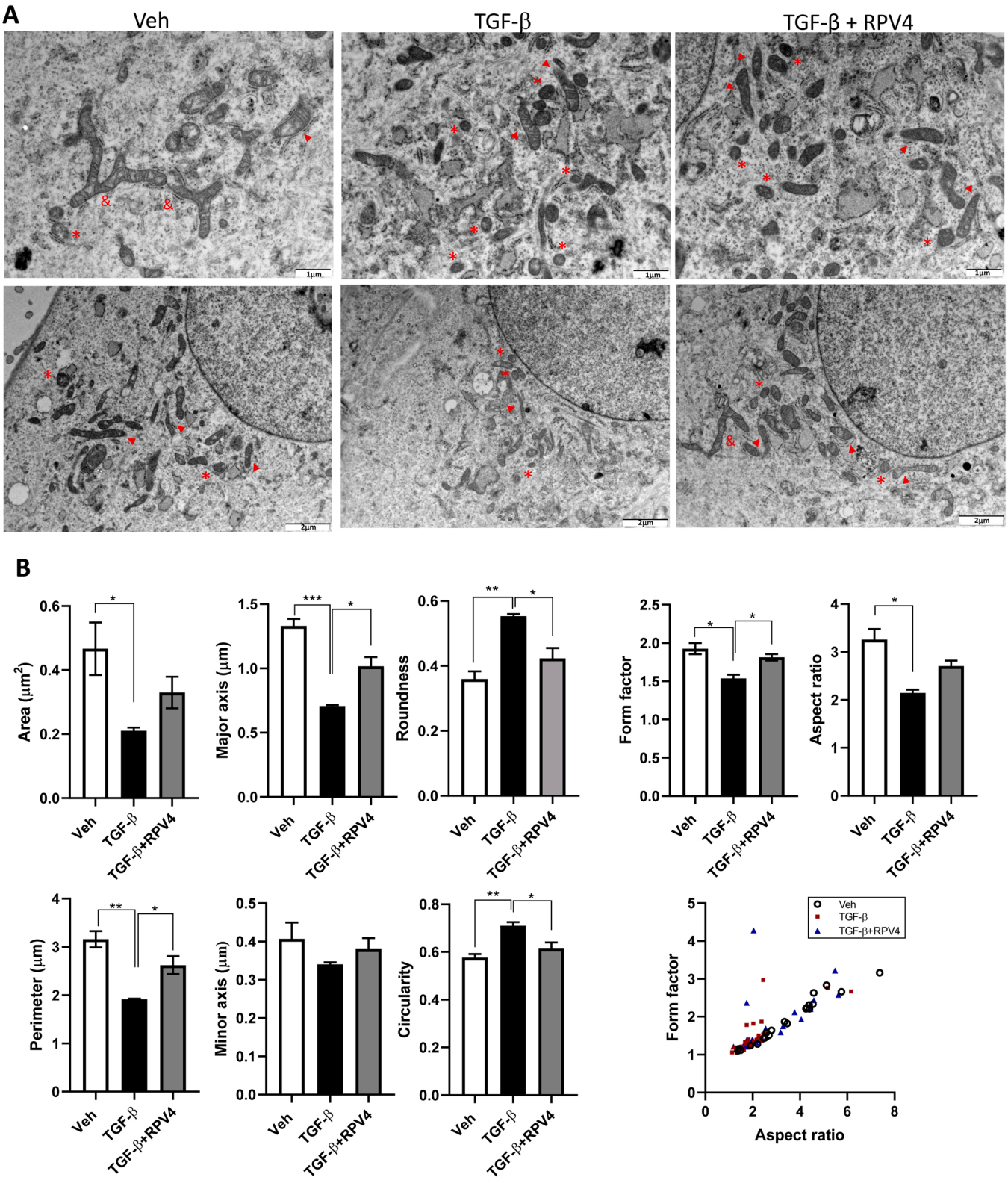

Fig. 5. Analysis of mitochondrial shape and size by transmission electron microscopy. LX2 cells were treated for 48 h with Vehicle (Veh), TGF-β alone or TGF-β in the presence of 4 μM RPV. Representative images (A) and quantification of data (by Image J) regarding mitochondrial shape and size descriptors (area, perimeter, major axis, minor axis, circularity, roundness, form factor and aspect ratio) of an individual mitochondrion (B) are shown. The results are expressed as the mean±SEM of at least 50 mitochondria per condition (4–5 images per condition), except for "aspect ratio vs form factor plot", which shows mitochondria individually studied in one independent experiment. Data (n=3) were statistically analyzed by an unpaired Student's t-test of TGF-β vs Veh or TGF-β+RPV4 vs TGF-β (*, ** and *** represent a *p* value <0.05, <0.01 or <0.001 respectively). * round mitochondria, Δ elongated mitochondria, & branched mitochondria.

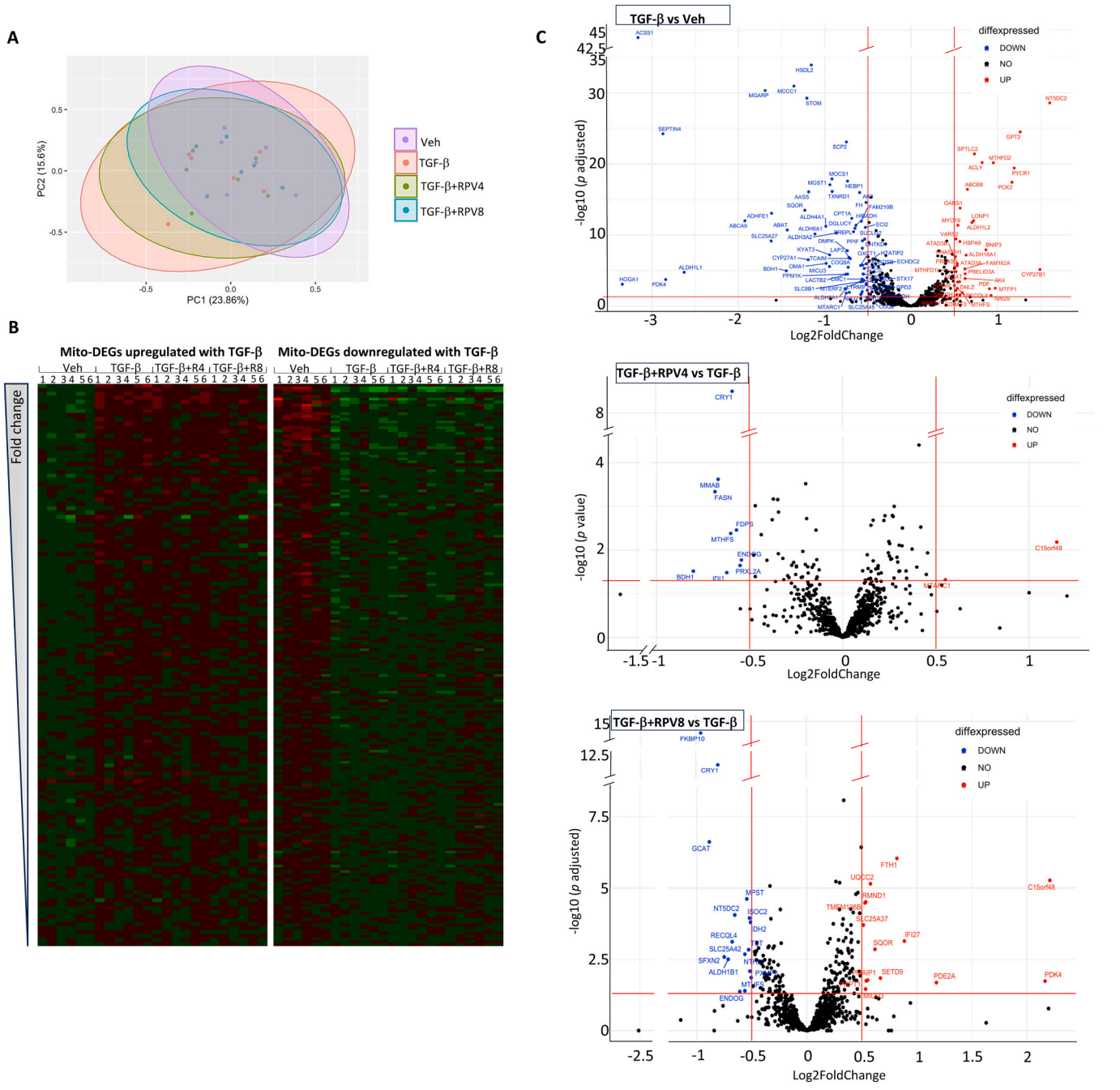

Fig. 6. RNA sequencing analysis of mito-DEGs (I). Primary human HSCs were treated with Vehicle (Veh), TGF-β alone or in presence of RPV (4 or 8 μM) (n=6). A total of 13,157 sequences were detected, of which 13,156 were protein-coding genes and sequences were filtered for genes encoding mitochondrial proteins (mito-DEGs). (A) Principal component analysis (PCA) of the mito-DEGs in the four groups: TGF-β vs Veh, TGF-β+RPV4 vs TGF-β, TGF-β+RPV8 vs TGF-β and TGF-β-RPV8 vs TGF-β+RPV4. Variables 1 and 2 together explain 39.46 % of the total variance. (B) Heat maps showing the mito-DEGs which were upregulated (left) or down-regulated (right) in TGF-β-treated cells vs Veh, listed according to the fold change of the gene expression. (C) Volcano plots with the following comparisons: TGF-β vs Veh, TGF-β+RPV4 vs TGF-β and TGF-β+RPV8 vs TGF-β.

with MitoView and mitochondrial branching was quantified. We observed that 48 h-treatment with TGF-β led to a significant decrease in the length of the mitochondrial branches, an effect that was rescued in the cells co-exposed to RPV 4 μM (Fig. 4A, B). This result suggested alterations of mitochondrial dynamics, a term that refers to the changing process of mitochondrial fission and fusion. Several protein markers of these processes were evaluated by western blot in cells exposed to TGF-β, alone or in the presence of RPV (2,4 or 8 μM). Upon exposure to TGF-β, we did not observe changes in the levels of OPA1 (optic atrophy gene 1) or MFN2 (mitofusin 2), proteins that regulate mitochondrial fusion. On the contrary, TGF-β enhanced the protein content of the phosphorylated form of DRP1 (dynamin-related protein 1), a GTPase that regulates mitochondrial fission. The highest concentration of RPV employed (8 μM) led to a decrease in pDRP1 levels in TGF-β-exposed cells (Fig. 4C, D). In summary, activation of LX2 cells with TGF-β altered the normal mitochondrial network and enhanced the presence of fissioned mitochondria, effects that were ameliorated by the presence of RPV.

We also performed morphometric TEM image analysis of mitochondria in these cells. Mitochondria are typically round-to-oval in shape and range in size from 0.5 to 10 μm according to cell type and

Table 1
Differential expression analysis of genes encoding mitochondrial proteins (mito-DEGs) using RNA sequencing data of TGF-β-activated-HSCs versus treatment with vehicle. Upregulated and downregulated mito-DEGs are shown. Primary human HSCs were treated with vehicle or TGF-β for 48 h (n=6), adjusted p<0.05. Genesare listed according to the value of FC (Fold change).

TGF-β vs Veh UPREGULATED				
hgnc_symbol	**Description**	**HGNC Symbol. Acc.**	**log2FC**	**adjusted p**
NT5DC2	5'-nucleotidase domain containing 2	HGNC:25717	1.606	2.59E−29
CYP27B1	cytochrome P450 family 27 subfamily B member 1	HGNC:2606	1.491	7.33E−06
GPT2	glutamic-pyruvic transaminase 2	HGNC:18062	1.263	3.10E−25
PYCR1	pyrroline−5-carboxylate reductase 1	HGNC:9721	1.193	3.91E−20
PCK2	phosphoenolpyruvate carboxykinase 2, mitochondrial	HGNC:8725	1.168	3.80E−18
MTFP1	mitochondrial fission process 1	HGNC:26945	0.973	3.18E−03
MTHFD2	methylenetetrahydrofolate dehydrogenase (NADP+ dependent) 2, methenyltetrahydrofolate cyclohydrolase	HGNC:7434	0.952	6.87E−21
NAGS	N-acetylglutamate synthase	HGNC:17996	0.925	3.41E−02
PDF	peptide deformylase, mitochondrial	HGNC:30012	0.906	3.77E−03
BNIP3	BCL2 interacting protein 3	HGNC:1084	0.866	1.22E−08
ACLY	ATP citrate lyase	HGNC:115	0.822	6.54E−21
SPTLC2	serine palmitoyltransferase long chain base subunit 2	HGNC:11278	0.733	3.84E−22
LONP1	lon peptidase 1, mitochondrial	HGNC:9479	0.723	9.85E−13
ALDH1L2	aldehyde dehydrogenase 1 family member L2	HGNC:26777	0.704	1.75E−12
ABCB8	ATP binding cassette subfamily B member 8	HGNC:49	0.652	3.81E−17
ALDH18A1	aldehyde dehydrogenase 18 family member A1	HGNC:9722	0.637	6.96E−08
PRELID3A	PRELI domain containing 3 A	HGNC:24639	0.626	2.96E−05
AK4	adenylate kinase 4	HGNC:363	0.625	1.33E−04
FAM162A	family with sequence similarity 162 member A	HGNC:17865	0.622	6.04E−06
MTHFS	methenyltetrahydrofolate synthetase	HGNC:7437	0.591	1.31E−02
GARS1	glycyl-tRNA synthetase 1	HGNC:4162	0.568	1.65E−14
SDHAF3	succinate dehydrogenase complex assembly factor 3	HGNC:21752	0.565	2.85E−02
HSPA9	heat shock protein family A (Hsp70) member 9	HGNC:5244	0.565	8.40E−10
DNLZ	DNL-type zinc finger	HGNC:33879	0.561	3.87E−04
MYO19	myosin XIX	HGNC:26234	0.542	4.37E−12
AADAT	aminoadipate aminotransferase	HGNC:17929	0.538	4.39E−04
RECQL4	RecQ like helicase 4	HGNC:9949	0.535	3.19E−03
ATAD3A	ATPase family AAA domain containing 3A	HGNC:25567	0.534	2.04E−06
ATAD3B	ATPase family AAA domain containing 3B	HGNC:24007	0.534	1.06E−06
MARS2	methionyl-tRNA synthetase 2, mitochondrial	HGNC:25133	0.528	2.63E−02
MTHFD1L	methylenetetrahydrofolate dehydrogenase (NADP+ dependent) 1 like	HGNC:21055	0.520	1.46E−05
VARS2	valyl-tRNA synthetase 2, mitochondrial	HGNC:21642	0.519	3.66E−10
SARDH	sarcosine dehydrogenase	HGNC:10536	0.518	6.47E−03
RNASEH1	ribonuclease H1	HGNC:18466	0.513	1.10E−07
PRDX5	peroxiredoxin 5	HGNC:9355	0.506	3.73E−06
GPAM	glycerol−3-phosphate acyltransferase, mitochondrial	HGNC:24865	0.501	1.31E−03
CMC2	C-X9-C motif containing 2	HGNC:24447	0.500	5.06E−06
PAM16	presequence translocase associated motor 16	HGNC:29679	0.489	3.14E−04
HDHD5	haloacid dehalogenase like hydrolase domain containing 5	HGNC:1843	0.482	1.06E−04
MPV17L2	MPV17 mitochondrial inner membrane protein like 2	HGNC:28177	0.480	5.93E−05
AHCYL1	adenosylhomocysteinase like 1	HGNC:344	0.477	5.38E−08
FKBP10	FKBP prolyl isomerase 10	HGNC:18169	0.472	6.88E−05
PUS1	pseudouridine synthase 1	HGNC:15508	0.471	1.71E−05
ISOC2	isochorismatase domain containing 2	HGNC:26278	0.463	1.33E−04
GTPBP3	GTP binding protein 3, mitochondrial	HGNC:14880	0.458	3.37E−03
COQ4	coenzyme Q4	HGNC:19693	0.428	1.47E−05
MRPL17	mitochondrial ribosomal protein L17	HGNC:14053	0.427	4.36E−04
SHMT2	serine hydroxymethyltransferase 2	HGNC:10852	0.413	7.04E−10
TOMM40	translocase of outer mitochondrial membrane 40	HGNC:18001	0.412	1.64E−05
PLSCR3	phospholipid scramblase 3	HGNC:16495	0.410	2.40E−05
TIMM44	translocase of inner mitochondrial membrane 44	HGNC:17316	0.409	4.19E−07
PRELID3B	PRELI domain containing 3B	HGNC:15892	0.406	2.16E−04
MRPL52	mitochondrial ribosomal protein L52	HGNC:16655	0.405	9.89E−06
PET117	PET117 cytochrome c oxidase chaperone	HGNC:40045	0.402	4.04E−02
ACADVL	acyl-CoA dehydrogenase very long chain	HGNC:92	0.401	1.65E−04
POLRMT	RNA polymerase mitochondrial	HGNC:9200	0.399	9.93E−07
AURKAIP1	aurora kinase A interacting protein 1	HGNC:24114	0.397	1.14E−05
LIG3	DNA ligase 3	HGNC:6600	0.395	3.54E−07
UQCRC1	ubiquinol-cytochrome c reductase core protein 1	HGNC:12585	0.393	1.45E−07
CPOX	coproporphyrinogen oxidase	HGNC:2321	0.391	3.33E−04
GRPEL2	GrpE like 2, mitochondrial	HGNC:21060	0.384	5.25E−03
AK2	adenylate kinase 2	HGNC:362	0.382	3.49E−06
FLAD1	flavin adenine dinucleotide synthetase 1	HGNC:24671	0.377	4.27E−04
MTFR1	mitochondrial fission regulator 1	HGNC:29510	0.377	1.13E−03
ECI1	enoyl-CoA delta isomerase 1	HGNC:2703	0.369	3.54E−04
PAICS	phosphoribosylaminoimidazole carboxylase and phosphoribosylaminoimidazolesuccinocarboxamide synthase	HGNC:8587	0.364	1.79E−02
PRELID1	PRELI domain containing 1	HGNC:30255	0.363	3.22E−05
FAM210A	family with sequence similarity 210 member A	HGNC:28346	0.362	1.38E−02
POLG	DNA polymerase gamma, catalytic subunit	HGNC:9179	0.355	1.00E−07
CHCHD6	coiled-coil-helix-coiled-coil-helix domain containing 6	HGNC:28184	0.352	3.48E−02
PUSL1	pseudouridine synthase like 1	HGNC:26914	0.350	4.42E−03

(*continued on next page*)

Table 1 (*continued*)

TGF-β vs Veh UPREGULATED				
hgnc_symbol	**Description**	**HGNC Symbol. Acc.**	**log2FC**	**adjusted p**
COQ10A	coenzyme Q10A	HGNC:26515	0.348	4.72E−02
MRPL37	mitochondrial ribosomal protein L37	HGNC:14034	0.347	1.87E−03
SFXN4	sideroflexin 4	HGNC:16088	0.346	1.52E−02
FOXRED1	FAD dependent oxidoreductase domain containing 1	HGNC:26927	0.345	2.86E−03
NOCT	nocturnin	HGNC:14254	0.338	4.45E−02
MRPL2	mitochondrial ribosomal protein L2	HGNC:14056	0.336	1.98E−03
TRMT1	tRNA methyltransferase 1	HGNC:25980	0.335	7.42E−04
FASTK	Fas activated serine/threonine kinase	HGNC:24676	0.333	1.07E−05
CHCHD2	coiled-coil-helix-coiled-coil-helix domain containing 2	HGNC:21645	0.324	8.42E−04
HINT3	histidine triad nucleotide binding protein 3	HGNC:18468	0.323	7.57E−03
TRMU	tRNA mitochondrial 2-thiouridylase	HGNC:25481	0.322	2.00E−03
COX10	cytochrome c oxidase assembly factor heme A:farnesyltransferase COX10	HGNC:2260	0.322	1.84E−02
BAK1	BCL2 antagonist/killer 1	HGNC:949	0.322	1.86E−03
GHITM	growth hormone inducible transmembrane protein	HGNC:17281	0.321	1.73E−08
TIMM21	translocase of inner mitochondrial membrane 21	HGNC:25010	0.314	2.96E−02
MPST	mercaptopyruvate sulfurtransferase	HGNC:7223	0.314	9.79E−03
HAGH	hydroxyacylglutathione hydrolase	HGNC:4805	0.312	3.38E−03
FAHD1	fumarylacetoacetate hydrolase domain containing 1	HGNC:14169	0.312	3.23E−04
DNAJA3	DnaJ heat shock protein family (Hsp40) member A3	HGNC:11808	0.309	9.12E−08
NME6	NME/NM23 nucleoside diphosphate kinase 6	HGNC:20567	0.307	1.11E−02
ACAA2	acetyl-CoA acyltransferase 2	HGNC:83	0.305	1.25E−03
HINT2	histidine triad nucleotide binding protein 2	HGNC:18344	0.305	4.07E−02
BBC3	BCL2 binding component 3	HGNC:17868	0.302	1.45E−02
MRPL18	mitochondrial ribosomal protein L18	HGNC:14477	0.301	6.20E−04
HEMK1	HemK methyltransferase family member 1	HGNC:24923	0.294	2.22E−03
TIMM13	translocase of inner mitochondrial membrane 13	HGNC:11816	0.291	7.64E−03
CRY1	cryptochrome circadian regulator 1	HGNC:2384	0.287	8.81E−03
HTRA2	HtrA serine peptidase 2	HGNC:14348	0.287	6.17E−03
MRPS26	mitochondrial ribosomal protein S26	HGNC:14045	0.284	2.56E−02
SLC25A32	solute carrier family 25 member 32	HGNC:29683	0.283	1.68E−02
TWNK	twinkle mtDNA helicase	HGNC:1160	0.283	4.63E−02
CYCS	cytochrome c, somatic	HGNC:19986	0.282	7.22E−03
SDHB	succinate dehydrogenase complex iron sulfur subunit B	HGNC:10681	0.280	9.26E−04
HSPD1	heat shock protein family D (Hsp60) member 1	HGNC:5261	0.277	1.47E−02
MRRF	mitochondrial ribosome recycling factor	HGNC:7234	0.273	2.12E−03
PPOX	protoporphyrinogen oxidase	HGNC:9280	0.273	4.30E−02
TRIT1	tRNA isopentenyltransferase 1	HGNC:20286	0.268	4.19E−02
TFB2M	transcription factor B2, mitochondrial	HGNC:18559	0.258	3.09E−02
NDUFB7	NADH:ubiquinone oxidoreductase subunit B7	HGNC:7702	0.256	2.81E−02
COX7A2L	cytochrome c oxidase subunit 7A2 like	HGNC:2289	0.249	1.48E−03
MTG1	mitochondrial ribosome associated GTPase 1	HGNC:32159	0.248	1.55E−02
NGRN	neugrin, neurite outgrowth associated	HGNC:18077	0.246	4.29E−03
GSR	glutathione-disulfide reductase	HGNC:4623	0.240	2.63E−02
ABHD10	abhydrolase domain containing 10, depalmitoylase	HGNC:25656	0.236	3.98E−02
TBRG4	transforming growth factor beta regulator 4	HGNC:17443	0.234	3.42E−03
GOLPH3	golgi phosphoprotein 3	HGNC:15452	0.231	4.79E−03
MRPS12	mitochondrial ribosomal protein S12	HGNC:10380	0.226	3.59E−02
FECH	ferrochelatase	HGNC:3647	0.224	4.07E−02
DUT	deoxyuridine triphosphatase	HGNC:3078	0.220	1.56E−02
RHOT2	ras homolog family member T2	HGNC:21169	0.215	1.79E−02
MSRB3	methionine sulfoxide reductase B3	HGNC:27375	0.214	5.73E−03
MRM2	mitochondrial rRNA methyltransferase 2	HGNC:16352	0.212	3.09E−02
NDUFA8	NADH:ubiquinone oxidoreductase subunit A8	HGNC:7692	0.211	4.95E−02
COQ9	coenzyme Q9	HGNC:25302	0.209	1.01E−02
PHB2	prohibitin 2	HGNC:30306	0.207	2.68E−03
CYC1	cytochrome c1	HGNC:2579	0.203	2.60E−02
PDPR	pyruvate dehydrogenase phosphatase regulatory subunit	HGNC:30264	0.200	6.83E−03
BNIP3L	BCL2 interacting protein 3 like	HGNC:1085	0.195	1.76E−02
C1QBP	complement C1q binding protein	HGNC:1243	0.192	4.48E−02
TIMM50	translocase of inner mitochondrial membrane 50	HGNC:23656	0.192	4.60E−02
TIMM17A	translocase of inner mitochondrial membrane 17A	HGNC:17315	0.187	1.87E−02
MIEF1	mitochondrial elongation factor 1	HGNC:25979	0.187	1.09E−02
PYCR2	pyrroline−5-carboxylate reductase 2	HGNC:30262	0.186	2.88E−02
OAT	ornithine aminotransferase	HGNC:8091	0.168	8.53E−03
LETM1	leucine zipper and EF-hand containing transmembrane protein 1	HGNC:6556	0.164	2.17E−02
NSUN2	NOP2/Sun RNA methyltransferase 2	HGNC:25994	0.133	3.75E−02
SND1	staphylococcal nuclease and tudor domain containing 1	HGNC:30646	0.127	4.46E−02
DLST	dihydrolipoamide S-succinyltransferase	HGNC:2911	0.116	3.39E−02
TGF-β vs Veh DOWNREGULATED				
hgnc_symbol	**Description**	**HGNC Symbol. Acc.**	**log2FC**	**adjusted p**
HOGA1	4-hydroxy−2-oxoglutarate aldolase 1	HGNC:25155	−3.344	8.79E−04
ACSS1	acyl-CoA synthetase short chain family member 1	HGNC:16091	−3.163	1.20E−44

(*continued on next page*)

Table 1 (*continued*)

TGF-β vs Veh DOWNREGULATED				
hgnc_symbol	**Description**	**HGNC Symbol. Acc.**	**log2FC**	**adjusted p**
SEPTIN4	septin 4	HGNC:9165	−2.874	5.82E−25
PDK4	pyruvate dehydrogenase kinase 4	HGNC:8812	−2.842	1.89E−04
ALDH1L1	aldehyde dehydrogenase 1 family member L1	HGNC:3978	−2.628	1.81E−05
ABCA9	ATP binding cassette subfamily A member 9	HGNC:39	−1.925	1.02E−12
MGARP	mitochondria localized glutamic acid rich protein	HGNC:29969	−1.691	4.61E−31
SLC25A27	solute carrier family 25 member 27	HGNC:21065	−1.621	7.07E−10
ADHFE1	alcohol dehydrogenase iron containing 1	HGNC:16354	−1.616	8.84E−14
BDH1	3-hydroxybutyrate dehydrogenase 1	HGNC:1027	−1.445	1.12E−05
ABAT	4-aminobutyrate aminotransferase	HGNC:23	−1.434	2.04E−11
MCCC1	methylcrotonyl-CoA carboxylase subunit 1	HGNC:6936	−1.357	1.10E−31
SQOR	sulfide quinone oxidoreductase	HGNC:20390	−1.231	3.35E−14
STOM	stomatin	HGNC:3383	−1.208	5.48E−30
CYP27A1	cytochrome P450 family 27 subfamily A member 1	HGNC:2605	−1.192	3.07E−07
AASS	aminoadipate-semialdehyde synthase	HGNC:17366	−1.186	8.49E−17
HSDL2	hydroxysteroid dehydrogenase like 2	HGNC:18572	−1.156	1.19E−34
ALDH6A1	aldehyde dehydrogenase 6 family member A1	HGNC:7179	−1.114	7.32E−11
ALDH4A1	aldehyde dehydrogenase 4 family member A1	HGNC:406	−0.987	6.18E−12
OMA1	OMA1 zinc metallopeptidase	HGNC:29661	−0.984	1.01E−06
MICU3	mitochondrial calcium uptake family member 3	HGNC:27820	−0.946	2.80E−06
KYAT3	kynurenine aminotransferase 3	HGNC:33238	−0.944	6.46E−08
MGST1	microsomal glutathione S-transferase 1	HGNC:7061	−0.941	8.58E−18
MOCS1	molybdenum cofactor synthesis 1	HGNC:7190	−0.917	1.29E−18
TXNRD1	thioredoxin reductase 1	HGNC:12437	−0.915	7.52E−17
ALDH3A2	aldehyde dehydrogenase 3 family member A2	HGNC:403	−0.866	5.34E−11
ALDH5A1	aldehyde dehydrogenase 5 family member A1	HGNC:408	−0.759	4.14E−03
PPM1K	protein phosphatase, Mg2+/Mn2+ dependent 1 K	HGNC:25415	−0.755	3.40E−05
MTARC1	mitochondrial amidoxime reducing component 1	HGNC:26189	−0.751	1.57E−02
SCP2	sterol carrier protein 2	HGNC:10606	−0.749	8.11E−24
DMPK	DM1 protein kinase	HGNC:2933	−0.738	1.65E−08
HEBP1	heme binding protein 1	HGNC:17176	−0.735	2.64E−18
LACTB2	lactamase beta 2	HGNC:18512	−0.735	3.25E−05
COQ8A	coenzyme Q8A	HGNC:16812	−0.728	3.55E−06
LAP3	leucine aminopeptidase 3	HGNC:18449	−0.720	1.50E−07
ARG2	arginase 2	HGNC:664	−0.716	1.23E−02
TCAIM	T cell activation inhibitor, mitochondrial	HGNC:25241	−0.704	2.16E−07
CPT1A	carnitine palmitoyltransferase 1 A	HGNC:2328	−0.687	4.65E−13
PREPL	prolyl endopeptidase like	HGNC:30228	−0.667	3.50E−11
DGLUCY	D-glutamate cyclase	HGNC:20498	−0.649	1.13E−11
HIBADH	3-hydroxyisobutyrate dehydrogenase	HGNC:4907	−0.638	4.32E−12
AK3	adenylate kinase 3	HGNC:17376	−0.596	1.08E−16
OXCT1	3-oxoacid CoA-transferase 1	HGNC:8527	−0.584	1.93E−06
MTERF2	mitochondrial transcription termination factor 2	HGNC:30779	−0.582	3.94E−04
SLC25A45	solute carrier family 25 member 45	HGNC:27442	−0.582	2.39E−02
FAM210B	family with sequence similarity 210 member B	HGNC:16102	−0.576	1.17E−12
SETD9	SET domain containing 9	HGNC:28508	−0.575	1.91E−02
CMC1	C-X9-C motif containing 1	HGNC:28783	−0.567	1.58E−04
LYRM9	LYR motif containing 9	HGNC:27314	−0.566	9.45E−03
DHTKD1	dehydrogenase E1 and transketolase domain containing 1	HGNC:23537	−0.564	7.48E−09
PPIF	peptidylprolyl isomerase F	HGNC:9259	−0.563	6.60E−10
ACADSB	acyl-CoA dehydrogenase short/branched chain	HGNC:91	−0.561	1.82E−06
SLC8B1	solute carrier family 8 member B1	HGNC:26175	−0.557	3.41E−04
ACCS	1-aminocyclopropane−1-carboxylate synthase homolog (inactive)	HGNC:23989	−0.556	3.07E−05
STX17	syntaxin 17	HGNC:11432	−0.550	3.22E−05
GPD2	glycerol−3-phosphate dehydrogenase 2	HGNC:4456	−0.547	2.39E−04
ECHDC2	enoyl-CoA hydratase domain containing 2	HGNC:23408	−0.542	5.04E−06
SUCLG2	succinate-CoA ligase GDP-forming subunit beta	HGNC:11450	−0.537	3.91E−10
ECI2	enoyl-CoA delta isomerase 2	HGNC:14601	−0.529	8.86E−12
FH	fumarate hydratase	HGNC:3700	−0.521	2.68E−15
EHHADH	enoyl-CoA hydratase and 3-hydroxyacyl CoA dehydrogenase	HGNC:3247	−0.520	1.04E−03
HTATIP2	HIV−1 Tat interactive protein 2	HGNC:16637	−0.519	1.17E−06
DMAC2L	distal membrane arm assembly component 2 like	HGNC:18799	−0.518	6.85E−04
MTARC2	mitochondrial amidoxime reducing component 2	HGNC:26064	−0.509	1.01E−04
COQ2	coenzyme Q2, polyprenyltransferase	HGNC:25223	−0.507	6.00E−03
MRPS24	mitochondrial ribosomal protein S24	HGNC:14510	−0.499	1.20E−07
SLC25A29	solute carrier family 25 member 29	HGNC:20116	−0.490	1.94E−02
MGST3	microsomal glutathione S-transferase 3	HGNC:7064	−0.489	1.16E−09
DECR1	2,4-dienoyl-CoA reductase 1	HGNC:2753	−0.485	1.75E−12
GSTK1	glutathione S-transferase kappa 1	HGNC:16906	−0.483	4.34E−07
SFXN2	sideroflexin 2	HGNC:16086	−0.470	2.29E−02
UQCC1	ubiquinol-cytochrome c reductase complex assembly factor 1	HGNC:15891	−0.463	5.06E−16
PPA2	inorganic pyrophosphatase 2	HGNC:28883	−0.462	2.11E−05
ETFDH	electron transfer flavoprotein dehydrogenase	HGNC:3483	−0.451	1.57E−06
SLC25A1	solute carrier family 25 member 1	HGNC:10979	−0.451	1.02E−02
MSRA	methionine sulfoxide reductase A	HGNC:7377	−0.447	2.36E−04

(*continued on next page*)

Table 1 (*continued*)

TGF-β vs Veh DOWNREGULATED				
hgnc_symbol	**Description**	**HGNC Symbol. Acc.**	**log2FC**	**adjusted p**
PDP1	pyruvate dehydrogenase phosphatase catalytic subunit 1	HGNC:9279	−0.445	9.29E−05
ACAT1	acetyl-CoA acetyltransferase 1	HGNC:93	−0.441	2.38E−07
CAT	catalase	HGNC:1516	−0.440	3.41E−06
BCL2L1	BCL2 like 1	HGNC:992	−0.437	8.27E−05
OSBPL1A	oxysterol binding protein like 1A	HGNC:16398	−0.436	8.48E−05
NDUFC1	NADH:ubiquinone oxidoreductase subunit C1	HGNC:7705	−0.435	1.63E−05
SPR	sepiapterin reductase	HGNC:11257	−0.432	1.67E−03
HIGD1A	HIG1 hypoxia inducible domain family member 1A	HGNC:29527	−0.431	4.67E−02
DHRS7B	dehydrogenase/reductase 7B	HGNC:24547	−0.428	1.23E−03
PDP2	pyruvate dehydrogenase phosphatase catalytic subunit 2	HGNC:30263	−0.426	3.10E−03
PNKD	PNKD metallo-beta-lactamase domain containing	HGNC:9153	−0.415	1.87E−04
IVD	isovaleryl-CoA dehydrogenase	HGNC:6186	−0.411	2.73E−07
WARS2	tryptophanyl tRNA synthetase 2, mitochondrial	HGNC:12730	−0.410	6.40E−03
MMUT	methylmalonyl-CoA mutase	HGNC:7526	−0.410	1.15E−06
PNPO	pyridoxamine 5′-phosphate oxidase	HGNC:30260	−0.408	2.07E−03
HSD17B4	hydroxysteroid 17-beta dehydrogenase 4	HGNC:5213	−0.405	2.42E−11
NDUFV2	NADH:ubiquinone oxidoreductase core subunit V2	HGNC:7717	−0.405	4.13E−04
PC	pyruvate carboxylase	HGNC:8636	−0.404	1.24E−02
MRPS6	mitochondrial ribosomal protein S6	HGNC:14051	−0.390	2.14E−04
CROT	carnitine O-octanoyltransferase	HGNC:2366	−0.389	4.25E−03
SLC25A30	solute carrier family 25 member 30	HGNC:27371	−0.386	1.93E−02
NBR1	NBR1 autophagy cargo receptor	HGNC:6746	−0.383	1.64E−10
RMDN1	regulator of microtubule dynamics 1	HGNC:24285]	−0.382	4.18E−07
TEFM	transcription elongation factor, mitochondrial	HGNC:26223]	−0.379	1.80E−02
TXNRD2	thioredoxin reductase 2	HGNC:18155	−0.377	3.29E−06
MFF	mitochondrial fission factor	HGNC:24858	−0.377	1.48E−10
ACSS3	acyl-CoA synthetase short chain family member 3	HGNC:24723	−0.375	1.87E−02
PLPBP	pyridoxal phosphate binding protein	HGNC:9457	−0.374	9.57E−04
RMND1	required for meiotic nuclear division 1 homolog	HGNC:21176	−0.365	2.48E−03
LYRM4	LYR motif containing 4	HGNC:21365	−0.362	4.22E−05
MICU2	mitochondrial calcium uptake 2	HGNC:31830	−0.357	9.20E−04
NDUFA4	NDUFA4 mitochondrial complex associated	HGNC:7687	−0.355	2.39E−04
DNAJC15	DnaJ heat shock protein family (Hsp40) member C15	HGNC:20325	−0.355	8.79E−05
MTIF3	mitochondrial translational initiation factor 3	HGNC:29788	−0.354	9.96E−04
MPC1	mitochondrial pyruvate carrier 1	HGNC:21606	−0.353	6.84E−03
CASP8	caspase 8	HGNC:1509	−0.351	4.08E−03
MCCC2	methylcrotonyl-CoA carboxylase subunit 2	HGNC:6937	−0.350	2.64E−04
MRPL33	mitochondrial ribosomal protein L33	HGNC:14487	−0.342	1.35E−04
BCKDHB	branched chain keto acid dehydrogenase E1 subunit beta	HGNC:987	−0.339	4.73E−02
RHOT1	ras homolog family member T1	HGNC:21168	−0.338	8.81E−03
CARS2	cysteinyl-tRNA synthetase 2, mitochondrial	HGNC:25695	−0.337	3.53E−05
NNT	nicotinamide nucleotide transhydrogenase	HGNC:7863	−0.336	1.09E−04
GCDH	glutaryl-CoA dehydrogenase	HGNC:4189	−0.335	1.04E−02
ATPAF1	ATP synthase mitochondrial F1 complex assembly factor 1	HGNC:18803	−0.333	2.35E−05
ACSF2	acyl-CoA synthetase family member 2	HGNC:26101	−0.328	2.38E−02
HADHB	hydroxyacyl-CoA dehydrogenase trifunctional multienzyme complex subunit beta	HGNC:4803	−0.327	5.40E−10
MRPL44	mitochondrial ribosomal protein L44	HGNC:16650	−0.326	5.94E−04
NDUFB1	NADH:ubiquinone oxidoreductase subunit B1	HGNC:7695	−0.326	1.30E−03
MPV17	mitochondrial inner membrane protein MPV17	HGNC:7224	−0.318	1.31E−06
OXR1	oxidation resistance 1	HGNC:15822	−0.317	2.74E−02
SLC25A25	solute carrier family 25 member 25	HGNC:20663	−0.317	1.53E−03
MPC2	mitochondrial pyruvate carrier 2	HGNC:24515	−0.316	4.62E−04
UNG	uracil DNA glycosylase	HGNC:12572	−0.315	2.48E−02
ME3	malic enzyme 3	HGNC:6985	−0.313	6.87E−04
CISD1	CDGSH iron sulfur domain 1	HGNC:30880	−0.311	9.03E−03
MRPS14	mitochondrial ribosomal protein S14	HGNC:14049	−0.308	6.15E−03
METTL5	methyltransferase 5, N6-adenosine	HGNC:25006	−0.300	2.82E−02
HMGCL	3-hydroxy−3-methylglutaryl-CoA lyase	HGNC:5005	−0.298	5.35E−03
HADHA	hydroxyacyl-CoA dehydrogenase trifunctional multienzyme complex subunit alpha	HGNC:4801	−0.296	1.86E−09
LYRM2	LYR motif containing 2	HGNC:25229	−0.296	1.91E−03
NIPSNAP3A	nipsnap homolog 3A	HGNC:23619	−0.295	4.89E−03
COX7C	cytochrome c oxidase subunit 7 C	HGNC:2292	−0.294	4.48E−05
SDHC	succinate dehydrogenase complex subunit C	HGNC:10682	−0.292	8.08E−08
SDHA	succinate dehydrogenase complex flavoprotein subunit A	HGNC:10680	−0.287	4.75E−05
NFU1	NFU1 iron-sulfur cluster scaffold	HGNC:16287	−0.287	3.26E−03
COQ8B	coenzyme Q8B	HGNC:19041	−0.287	2.17E−02
TMEM126B	transmembrane protein 126B	HGNC:30883	−0.285	2.13E−02
COX15	cytochrome c oxidase assembly homolog COX15	HGNC:2263	−0.285	6.22E−05
CPS1	carbamoyl-phosphate synthase 1	HGNC:2323	−0.284	2.11E−02
UQCRB	ubiquinol-cytochrome c reductase binding protein	HGNC:12582	−0.278	2.95E−05
GATB	glutamyl-tRNA amidotransferase subunit B	HGNC:8849	−0.277	4.41E−03
ACAD10	acyl-CoA dehydrogenase family member 10	HGNC:21597	−0.276	1.07E−02
CYB5R3	cytochrome b5 reductase 3	HGNC:2873	−0.274	3.52E−03
RDH14	retinol dehydrogenase 14	HGNC:19979	−0.273	2.17E−02

(*continued on next page*)

Table 1 (*continued*)

TGF-β vs Veh DOWNREGULATED				
hgnc_symbol	**Description**	**HGNC Symbol. Acc.**	**log2FC**	**adjusted p**
PRDX2	peroxiredoxin 2	HGNC:9353	−0.273	2.48E−03
ATP5PD	ATP synthase peripheral stalk subunit d	HGNC:845	−0.271	4.52E−05
OCIAD1	OCIA domain containing 1	HGNC:16074	−0.270	7.64E−03
CCDC127	coiled-coil domain containing 127	HGNC:30520	−0.269	8.43E−03
MIPEP	mitochondrial intermediate peptidase	HGNC:7104	−0.266	8.86E−03
CPT2	carnitine palmitoyltransferase 2	HGNC:2330	−0.262	1.34E−02
AIFM2	apoptosis inducing factor mitochondria associated 2	HGNC:21411	−0.259	1.11E−02
EXD2	exonuclease 3′−5′ domain containing 2	HGNC:20217	−0.258	1.26E−02
HADH	hydroxyacyl-CoA dehydrogenase	HGNC:4799	−0.257	5.79E−03
MRPS27	mitochondrial ribosomal protein S27	HGNC:14512	−0.257	1.11E−04
IDE	insulin degrading enzyme	HGNC:5381	−0.255	1.41E−02
HIBCH	3-hydroxyisobutyryl-CoA hydrolase	HGNC:4908	−0.255	4.69E−02
NIPSNAP2	nipsnap homolog 2	HGNC:4179	−0.254	1.04E−02
OGDH	oxoglutarate dehydrogenase	HGNC:8124	−0.253	1.80E−03
PRORP	protein only RNase P catalytic subunit	HGNC:19958	−0.252	4.61E−02
CRYZ	crystallin zeta	HGNC:2419	−0.249	3.43E−02
TOMM70	translocase of outer mitochondrial membrane 70	HGNC:11985	−0.246	1.50E−02
NDUFS4	NADH:ubiquinone oxidoreductase subunit S4	HGNC:7711	−0.246	2.05E−03
DBT	dihydrolipoamide branched chain transacylase E2	HGNC:2698	−0.240	2.56E−02
SPHK2	sphingosine kinase 2	HGNC:18859	−0.237	1.64E−02
LACTB	lactamase beta	HGNC:16468	−0.236	3.37E−03
GLUD1	glutamate dehydrogenase 1	HGNC:4335	−0.233	1.00E−05
ECH1	enoyl-CoA hydratase 1	HGNC:3149	−0.233	4.14E−02
MCU	mitochondrial calcium uniporter	HGNC:23526	−0.233	4.17E−02
MAVS	mitochondrial antiviral signaling protein	HGNC:29233	−0.232	7.53E−04
ARL2	ADP ribosylation factor like GTPase 2	HGNC:693	−0.228	2.37E−02
NDUFB5	NADH:ubiquinone oxidoreductase subunit B5	HGNC:7700	−0.224	1.40E−02
LDHB	lactate dehydrogenase B	HGNC:6541	−0.223	2.78E−04
COQ5	coenzyme Q5, methyltransferase	HGNC:28722	−0.221	1.54E−02
PTCD3	pentatricopeptide repeat domain 3	HGNC:24717	−0.218	1.38E−02
CHCHD3	coiled-coil-helix-coiled-coil-helix domain containing 3	HGNC:21906	−0.218	3.21E−02
SAMM50	SAMM50 sorting and assembly machinery component	HGNC:24276	−0.214	3.60E−03
ATP5F1C	ATP synthase F1 subunit gamma	HGNC:833	−0.214	1.77E−03
ETFA	electron transfer flavoprotein subunit alpha	HGNC:3481	−0.214	3.36E−03
NIT2	nitrilase family member 2	HGNC:29878	−0.212	4.61E−03
BID	BH3 interacting domain death agonist	HGNC:1050	−0.211	4.78E−02
CASP3	caspase 3	HGNC:1504	−0.211	1.82E−02
PISD	phosphatidylserine decarboxylase	HGNC:8999	−0.209	7.07E−04
SDHD	succinate dehydrogenase complex subunit D	HGNC:10683	−0.201	1.68E−02
BCL2L13	BCL2 like 13	HGNC:17164	−0.199	2.50E−02
PEX11B	peroxisomal biogenesis factor 11 beta	HGNC:8853	−0.198	3.30E−02
AGK	acylglycerol kinase	HGNC:21869	−0.195	3.76E−02
ATP5MC2	ATP synthase membrane subunit c locus 2	HGNC:842	−0.163	3.59E−02
ACO2	aconitase 2	HGNC:118	−0.157	4.59E−02
IARS2	isoleucyl-tRNA synthetase 2, mitochondrial	HGNC:29685	−0.150	4.55E−02
ATP5F1A	ATP synthase F1 subunit alpha	HGNC:823	−0.149	4.73E−03
OXA1L	OXA1L mitochondrial inner membrane protein	HGNC:8526	−0.142	2.61E−02
SLC25A3	solute carrier family 25 member 3	HGNC:10989	−0.141	6.10E−03
TMEM14C	transmembrane protein 14 C	HGNC:20952	−0.127	3.61E−02

conditions. LX2 cells exposed to TGF-β exhibited smaller mitochondria with a rounder shape, and this effect was less noticeable when there was co-treatment with RPV 4 μM (Fig. 5). Mitochondrial surface and perimeter (both measures of mitochondrial size) were smaller when there was TGF-β treatment, and this was related to a decrease in the length of the major axis but not in that of the minor axis. Additionally, there was a reduction in the shape complexity/compactness, detected as a diminished value of form factor (the inverse ratio of the square perimeter of an object to the square perimeter of a circle of the same surface). We also quantified roundness and circularity, which are used to define how circular/round an object is. The data of these parameters, together with those of the aspect ratio (ratio between length and width), showed that TGF-β-treated cells had rounder mitochondria, while their shape tended to be more elongated after co-exposure to RPV. Altogether, the evidence obtained from TEM images is in line with the rest of the results showing that activation of LX2 cells with TGF-β altered the normal mitochondrial network and enhanced the presence of small and round mitochondria indicative of mitochondrial fission, effects that were ameliorated by the presence of RPV.

3.3. Study of the mitochondrial effect of RPV through RNA sequencing

To assess the effect of RPV on mitochondria in HSCs on a large scale, we performed RNA sequencing analysis using primary human HSCs exposed to Veh or TGF-β (alone or in the presence of RPV 4 μM or RPV 8 μM) for 48 h, which yielded expression data of 13,156 protein coding sequences. Next, we searched for the presence of genes coding for mitochondrial proteins among the DEGs identified in the study. To do this we employed MitoCarta 3.0 [26], a catalogue of 1036 human genes encoding mitochondrial proteome genes. 1016 of these genes were present in the results of the RNAseq study. The expression patterns were assessed through PCA (Fig. 6A). When cells exposed to TGF-β were compared to those treated with Veh, we detected 139 up-regulated and 199 down-regulated genes encoding mitochondrial proteins (mito--DEGs) (adjusted $p<0.05$) (Table 1). The expression patterns of these genes for each sample are shown in the heatmaps in Fig. 6B. We also analyzed the data through a volcano plot, a type of scatterplot that shows statistical significance (p value) versus magnitude of change (fold change) and thus enables quick visual identification of genes with large fold changes that are also statistically significant. This analysis revealed

Table 2
Differential expression analysis of genes encoding mitochondrial proteins (mito-DEGs) using RNA sequencing data of TGF-β+RPV4 vs TGF-β-activated-HSCs. Upregulated and downregulated mito-DEGs are shown. Primary human HSCs were treated with TGF-β alone or in the presence of 4 μM RPV for 48 h (n=6), $p<0.05$. Genes are listed according to the value of FC (Fold change).

TGF-β+RPV4 vs TGF-β UPREGULATED

hgnc_symbol	Description	HGNC Symbol. Acc.	log2FC	p
C15orf48	chromosome 15 open reading frame 48	HGNC:29898	1.149	6.60E−03
MTARC1	mitochondrial amidoxime reducing component 1	HGNC:26189	0.551	4.80E−02
PMAIP1	phorbol−12-myristate−13-acetate-induced protein 1	HGNC:9108	0.455	1.17E−02
IFI27	interferon alpha inducible protein 27	HGNC:5397	0.448	3.64E−02
FTH1	ferritin heavy chain 1	HGNC:3976	0.419	3.00E−03
FDXR	ferredoxin reductase	HGNC:3642	0.409	3.96E−05
CPT1B	carnitine palmitoyltransferase 1B	HGNC:2329	0.397	2.47E−02
ABHD11	abhydrolase domain containing 11	HGNC:16407	0.372	9.57E−03
C15orf61	chromosome 15 open reading frame 61	HGNC:34453	0.343	4.44E−02
NDUFAF4	NADH:ubiquinone oxidoreductase complex assembly factor 4	HGNC:21034	0.340	3.02E−02
RMND1	required for meiotic nuclear division 1 homolog	HGNC:21176	0.320	3.15E−03
TRMT61B	tRNA methyltransferase 61B	HGNC:26070	0.318	8.03E−03
CMC1	C-X9-C motif containing 1	HGNC:28783	0.305	3.02E−02
SLC25A37	solute carrier family 25 member 37	HGNC:29786	0.303	7.79E−03
ACSS3	acyl-CoA synthetase short chain family member 3	HGNC:24723	0.302	3.07E−02
ACSF2	acyl-CoA synthetase family member 2	HGNC:26101	0.295	1.90E−02
TRMT5	tRNA methyltransferase 5	HGNC:23141	0.291	1.47E−02
ALDH9A1	aldehyde dehydrogenase 9 family member A1	HGNC:412	0.276	1.01E−03
WARS2	tryptophanyl tRNA synthetase 2, mitochondrial	HGNC:12730	0.275	4.40E−02
HSPA9	heat shock protein family A (Hsp70) member 9	HGNC:5244	0.270	1.72E−03
ME3	malic enzyme 3	HGNC:6985	0.266	1.62E−03
UQCC2	ubiquinol-cytochrome c reductase complex assembly factor 2	HGNC:21237	0.262	1.59E−02
QRSL1	glutaminyl-tRNA amidotransferase subunit QRSL1	HGNC:21020	0.258	1.64E−02
DGLUCY	D-glutamate cyclase	HGNC:20498	0.252	7.14E−03
PPA2	inorganic pyrophosphatase 2	HGNC:28883	0.250	1.38E−02
MTO1	mitochondrial tRNA translation optimization 1	HGNC:19261	0.247	6.42E−03
XPNPEP3	X-prolyl aminopeptidase 3	HGNC:28052	0.245	1.16E−02
RMDN1	regulator of microtubule dynamics 1	HGNC:24285	0.227	1.64E−03
NDUFS4	NADH:ubiquinone oxidoreductase subunit S4	HGNC:7711	0.220	2.11E−03
HSDL2	hydroxysteroid dehydrogenase like 2	HGNC:18572	0.206	3.35E−02
SUPV3L1	Suv3 like RNA helicase	HGNC:11471	0.192	3.52E−02
SPIRE1	spire type actin nucleation factor 1	HGNC:30622	0.190	2.29E−02
NDUFA12	NADH:ubiquinone oxidoreductase subunit A12	HGNC:23987	0.189	2.66E−02
HEBP1	heme binding protein 1	HGNC:17176	0.189	2.37E−02
GFM2	GTP dependent ribosome recycling factor mitochondrial 2	HGNC:29682	0.178	4.72E−02
COQ5	coenzyme Q5, methyltransferase	HGNC:28722	0.177	2.74E−02
MRPS16	mitochondrial ribosomal protein S16	HGNC:14048	0.163	1.78E−02
GHITM	growth hormone inducible transmembrane protein	HGNC:17281	0.163	2.09E−03
GARS1	glycyl-tRNA synthetase 1	HGNC:4162	0.152	3.11E−02
HADHB	hydroxyacyl-CoA dehydrogenase trifunctional multienzyme complex subunit beta	HGNC:4803	0.152	2.73E−03
BAX	BCL2 associated X, apoptosis regulator	HGNC:959	0.149	4.77E−02
HINT1	histidine triad nucleotide binding protein 1	HGNC:4912	0.149	4.46E−02
COX7A2L	cytochrome c oxidase subunit 7A2 like	HGNC:2289	0.138	4.66E−02
ATP5PD	ATP synthase peripheral stalk subunit d	HGNC:845	0.136	2.66E−02
DNAJA3	DnaJ heat shock protein family (Hsp40) member A3	HGNC:11808	0.131	1.29E−02
DLD	dihydrolipoamide dehydrogenase	HGNC:2898	0.121	4.91E−02
NRDC	nardilysin convertase	HGNC:7995	0.107	3.01E−02

TGF-β+RPV4 vs TGF-β DOWNREGULATED

hgnc_symbol	Description	HGNC Symbol. Acc.	log2FC	p
BDH1	3-hydroxybutyrate dehydrogenase 1	HGNC:1027	−0.802	3.06E−02
FASN	fatty acid synthase	HGNC:3594	−0.686	4.62E−04
MMAB	metabolism of cobalamin associated B	HGNC:19331	−0.669	2.41E−04
IDI1	isopentenyl-diphosphate delta isomerase 1	HGNC:5387	−0.623	3.29E−02
MTHFS	methenyltetrahydrofolate synthetase	HGNC:7437	−0.602	4.19E−03
CRY1	cryptochrome circadian regulator 1	HGNC:2384	−0.591	3.24E−09
FDPS	farnesyl diphosphate synthase	HGNC:3631	−0.571	3.49E−03
PRXL2A	peroxiredoxin like 2A	HGNC:28651	−0.551	2.26E−02
ENDOG	endonuclease G	HGNC:3346	−0.544	1.70E−02
ALDH1B1	aldehyde dehydrogenase 1 family member B1	HGNC:407	−0.478	1.32E−02
GCAT	glycine C-acetyltransferase	HGNC:4188	−0.470	9.73E−04
ABAT	4-aminobutyrate aminotransferase	HGNC:23	−0.470	4.07E−02
SLC25A1	solute carrier family 25 member 1	HGNC:10979	−0.438	4.46E−03
PXMP4	peroxisomal membrane protein 4	HGNC:15920	−0.407	1.73E−02
SLC25A4	solute carrier family 25 member 4	HGNC:10990	−0.379	2.04E−03
MPV17L2	MPV17 mitochondrial inner membrane protein like 2	HGNC:28177	−0.373	6.81E−04
SLC25A23	solute carrier family 25 member 23	HGNC:19375	−0.349	7.02E−04
AADAT	aminoadipate aminotransferase	HGNC:17929	−0.346	1.22E−02
FKBP10	FKBP prolyl isomerase 10	HGNC:18169	−0.345	1.36E−03
TST	thiosulfate sulfurtransferase	HGNC:12388	−0.322	1.56E−02

(*continued on next page*)

Table 2 (*continued*)

TGF-β+RPV4 vs TGF-β DOWNREGULATED				
hgnc_symbol	**Description**	**HGNC Symbol. Acc.**	**log2FC**	**p**
RECQL4	RecQ like helicase 4	HGNC:9949	−0.317	4.81E−02
ALDH4A1	aldehyde dehydrogenase 4 family member A1	HGNC:406	−0.296	3.88E−02
PDK1	pyruvate dehydrogenase kinase 1	HGNC:8809	−0.289	4.29E−02
BOLA3	bolA family member 3	HGNC:24415	−0.274	2.24E−02
HDHD5	haloacid dehalogenase like hydrolase domain containing 5	HGNC:1843	−0.264	1.93E−02
MPC1	mitochondrial pyruvate carrier 1	HGNC:21606	−0.253	3.64E−02
ALDH18A1	aldehyde dehydrogenase 18 family member A1	HGNC:9722	−0.249	2.34E−02
IDH2	isocitrate dehydrogenase (NADP(+)) 2	HGNC:5383	−0.249	2.45E−02
SELENOO	selenoprotein O	HGNC:30395	−0.223	4.27E−02
MPST	mercaptopyruvate sulfurtransferase	HGNC:7223	−0.216	4.14E−02
ACLY	ATP citrate lyase	HGNC:115	−0.215	1.08E−02
DBI	diazepam binding inhibitor, acyl-CoA binding protein	HGNC:2690	−0.201	2.15E−02
SFXN3	sideroflexin 3	HGNC:16087	−0.199	3.05E−04
LETM1	leucine zipper and EF-hand containing transmembrane protein 1	HGNC:6556	−0.194	1.91E−03
ACACA	acetyl-CoA carboxylase alpha	HGNC:84	−0.188	2.43E−02
TOMM40	translocase of outer mitochondrial membrane 40	HGNC:18001	−0.186	3.37E−02
MYO19	myosin XIX	HGNC:26234	−0.165	2.51E−02
MSRB3	methionine sulfoxide reductase B3	HGNC:27375	−0.156	2.18E−02
PITRM1	pitrilysin metallopeptidase 1	HGNC:17663	−0.144	3.51E−03
BNIP3L	BCL2 interacting protein 3 like	HGNC:1085	−0.142	4.61E−02
PISD	phosphatidylserine decarboxylase	HGNC:8999	−0.140	1.67E−02
CYB5B	cytochrome b5 type B	HGNC:24374	−0.137	4.15E−02
PDHB	pyruvate dehydrogenase E1 subunit beta	HGNC:8808	−0.127	2.85E−02

major changes in the expression patterns of both up-regulated and down-regulated genes in cells treated with TGF-β compared to vehicle (Fig. 6C). The upregulated mito-DEGs with the greatest fold change and lowest *p* value were NT5DC2 (5′-nucleotidase domain containing 2), which has been widely associated with liver disease and is considered a novel prognostic marker in human hepatocellular carcinoma [27], and GPT2 (glutamic-pyruvic transaminase 2, also known as alanine aminotransaminase 1, ALT1). The downregulated mito-DEGs with the greatest fold change and lowest *p* value were acyl-CoA synthetase short chain family member 1 (ACSS1), a gene involved in lipid synthesis, and SEPTIN1, which has also been related to HSC activation in different ways [28,29]. Co-exposure to RPV 4 μM - in comparison with TGF-β alone - led to significantly altered mRNA levels of 90 mito-DEGs ($p<0.05$), of which 47 and 43 were up- and down-regulated, respectively (Table 2). Of these, 16 (34 %) of the significantly up-regulated and 15 (34.9 %) of the down-regulated mito-DEGs displayed reversed expression in regard to the mito-DEGs found in TGF-β-treated cells. Co-exposure to RPV 8 μM revealed the presence of 110 and 76 mito-DEGs, with significantly enhanced and diminished expression, respectively, with respect to exposure only to TGF-β (adjusted $p<0.05$) (Table 3). Of these, 49 (44.5 %) of the up-regulated and 31 (40.8 %) of the down-regulated mito-DEGs displayed reversed expression in regard to the mito-DEGs found in TGF-β-treated cells (Fig. 7A, B).

When we compared the mito-DEGs obtained by TGF-β+RPV4 with those obtained with TGF-β+RPV8, we detected that 35 up-regulated and 22 down-regulated mito-DEGs were common to both treatments (Fig. 8). We also compared the mito-DEGs from TGF-β+RPV4, which showed reversed expression compared to TGF-β alone vs those from TGF-β+RPV8, which displayed a reversed expression. We discovered the presence of 25 mito-DEGs; 12 of the 15 up-regulated and 13 of the 16 down-regulated mito-DEGs found in cells treated with TGF-β+RPV4 were also present when treatment consisted of TGF-β+RPV8 (Fig. 7A, B). According to MitoCarta 3.0, of these 25 mito-DEGs, 11 were described or predicted to be in the mitochondrial matrix, while the same could be said for 7 in the MIM, 2 in the MOM and 1 in IMS. In two cases the localization was defined as "unknown".

Our next objective was to assess which mitochondrial pathways were affected by co-treatment of TGF-β+RPV; specifically, the 12 up-regulated and 13 down-regulated mito-DEGs found in cells treated with TGF-β+RPV4 or TGF-β+RPV8 and which showed reversed expression compared to TGF-β. To do this, we analyzed "MitoPathways", which is part of the MitoCarta 3.0 DataSet, a database that includes 149 mitochondrial pathways with different hierarchies. 4 of the analyzed mito-DEGs (*CRY1*, *HDHD5*, *HSDL2* and *HEBP1*) were not found in the "MitoPathways" database, whereas the "MitoPathways Hierarchy" of the rest is shown in Table 4A and B. The pathways of higher hierarchy affected by RPV were "Mitochondrial central dogma", "Metabolism" and "OXPHOS" in the case of the up-regulated mito-DEGs and "Mitochondrial central dogma", "Metabolism", "Protein import, sorting and homeostasis", "Signaling" and "Mitochondrial dynamics and surveillance" in the case of the down-regulated mito-DEGs.

Finally, we also detected the presence of 5 (3.6 %) up-regulated and 6 (3.02 %) down-regulated Mito-DEGs in the cells under TGF-β treatment whose alteration was further enhanced after exposure to TGF-β+RPV4. The equivalent numbers in the case of TGF-β+RPV8 were 5 (3.6 %) and 8 (4 %) mito-DEGs.

4. Discussion

Despite major advances in our understanding of the pathogenesis of LF, and the urgent clinical need for its pharmacological treatment, the development of an effective, specific and curative antifibrotic drug is still pending. HSCs are a major cell type responsible for LF following their activation into fibrogenic myofibroblast-like cells. We have previously shown that the antiretroviral drug RPV is hepatoprotective and specifically interferes with LF development in different experimental scenarios, but which molecular processes participate in the deactivation of HSCs or in maintaining their quiescent state is yet to be defined. In the current follow-up research, we demonstrate that RPV blocks the mitochondrial effects produced by TGF-β in cultured HSCs. Importantly, the present research is an *in vitro* study, which has obvious limitations, and therefore our results cannot be directly extrapolated to clinical settings. Nevertheless, in addition to using the immortalized cell line LX2, we have employed primary cell cultures of freshly isolated human HSCs which mimic the physiological state of cells more closely, and this gives certain weight to our findings.

A vast number of studies have tackled the role of mitochondria in hepatocytes during CLD, but studies exploring the mitochondria in aHSCs in LF are fewer. In comparison to qHSCs, aHSCs display enhanced mitochondrial function, such as increased mitochondrial respiration (basal and maximal), ATP production, spare respiratory capacity, and, in some cases, proton leak [7,8,11]. aHSCs also exhibit positively regulated

Table 3
Differential expression analysis of genes encoding mitochondrial proteins (mito-DEGs) using RNA sequencing data of TGF-β+RPV8 vs TGF-β-activated-HSCs. Upregulated and downregulated mito-DEGs are shown. Primary human HSCs were treated with TGF-β alone or in the presence of 8 μM RPV for 48 h (n=6), adjusted p<0.05. Genes are listed according to the value of FC (Fold change).

TGF-β+RPV8 vs TGF-β UPREGULATED

hgnc_symbol	Description	HGNC Symbol. Acc.	log2FC	adjusted p
C15orf48	chromosome 15 open reading frame 48	HGNC:29898	2.210	5.38E−06
PDK4	pyruvate dehydrogenase kinase 4	HGNC:8812	2.166	1.84E−02
PDE2A	phosphodiesterase 2A	HGNC:8777	1.178	2.07E−02
IFI27	interferon alpha inducible protein 27	HGNC:5397	0.887	7.25E−04
FTH1	ferritin heavy chain 1	HGNC:3976	0.820	9.11E−07
SETD9	SET domain containing 9	HGNC:28508	0.669	1.44E−02
SQOR	sulfide quinone oxidoreductase	HGNC:20390	0.620	1.40E−03
UQCC2	ubiquinol-cytochrome c reductase complex assembly factor 2	HGNC:21237	0.579	7.09E−06
PMAIP1	phorbol−12-myristate−13-acetate-induced protein 1	HGNC:9108	0.553	1.69E−02
PNPT1	polyribonucleotide nucleotidyltransferase 1	HGNC:23166	0.541	1.80E−02
RMND1	required for meiotic nuclear division 1 homolog	HGNC:21176	0.536	3.07E−05
MICU3	mitochondrial calcium uptake family member 3	HGNC:27820	0.534	3.52E−02
TMEM126B	transmembrane protein 126B	HGNC:30883	0.529	3.31E−05
SLC25A37	solute carrier family 25 member 37	HGNC:29786	0.514	1.98E−04
SPIRE1	spire type actin nucleation factor 1	HGNC:30622	0.495	3.72E−07
MTERF2	mitochondrial transcription termination factor 2	HGNC:30779	0.486	1.19E−02
PPA2	inorganic pyrophosphatase 2	HGNC:28883	0.480	7.61E−05
SLC25A30	solute carrier family 25 member 30	HGNC:27371	0.477	8.46E−03
RHOT1	ras homolog family member T1	HGNC:21168	0.467	7.81E−04
SUPV3L1	Suv3 like RNA helicase	HGNC:11471	0.464	1.45E−05
KYAT3	kynurenine aminotransferase 3	HGNC:33238	0.459	3.50E−02
MTERF3	mitochondrial transcription termination factor 3	HGNC:24258	0.453	1.75E−02
HSPA9	heat shock protein family A (Hsp70) member 9	HGNC:5244	0.446	1.65E−05
FASTKD2	FAST kinase domains 2	HGNC:29160	0.431	4.97E−02
ACSS3	acyl-CoA synthetase short chain family member 3	HGNC:24723	0.429	1.61E−02
WARS2	tryptophanyl tRNA synthetase 2, mitochondrial	HGNC:12730	0.425	1.32E−02
ETFDH	electron transfer flavoprotein dehydrogenase	HGNC:3483	0.422	7.19E−05
PHYH	phytanoyl-CoA 2-hydroxylase	HGNC:8940	0.415	6.75E−03
TRIAP1	TP53 regulated inhibitor of apoptosis 1	HGNC:26937	0.412	1.55E−03
METTL15	methyltransferase like 15	HGNC:26606	0.411	2.63E−03
LRPPRC	leucine rich pentatricopeptide repeat containing	HGNC:15714	0.408	6.56E−04
MTARC2	mitochondrial amidoxime reducing component 2	HGNC:26064	0.406	8.31E−03
DGLUCY	D-glutamate cyclase	HGNC:20498	0.403	3.75E−04
MIPEP	mitochondrial intermediate peptidase	HGNC:7104	0.402	1.98E−04
MICU2	mitochondrial calcium uptake 2	HGNC:31830	0.401	7.94E−04
HADH	hydroxyacyl-CoA dehydrogenase	HGNC:4799	0.400	5.41E−05
TRMT5	tRNA methyltransferase 5	HGNC:23141	0.396	8.08E−03
MMAA	metabolism of cobalamin associated A	HGNC:18871	0.390	1.46E−02
TRMT10C	tRNA methyltransferase 10 C, mitochondrial RNase P subunit	HGNC:26022	0.386	9.73E−03
FDXR	ferredoxin reductase	HGNC:3642	0.384	1.91E−03
HSDL2	hydroxysteroid dehydrogenase like 2	HGNC:18572	0.376	1.56E−03
LYRM1	LYR motif containing 1	HGNC:25074	0.375	1.33E−03
LAP3	leucine aminopeptidase 3	HGNC:18449	0.373	2.51E−02
ME2	malic enzyme 2	HGNC:6984	0.369	4.47E−03
MGST1	microsomal glutathione S-transferase 1	HGNC:7061	0.365	6.43E−03
HEBP1	heme binding protein 1	HGNC:17176	0.365	2.93E−04
CHPT1	choline phosphotransferase 1	HGNC:17852	0.359	1.19E−02
ME3	malic enzyme 3	HGNC:6985	0.354	5.57E−04
PTRH2	peptidyl-tRNA hydrolase 2	HGNC:24265	0.351	5.92E−03
SLC25A13	solute carrier family 25 member 13	HGNC:10983	0.345	2.06E−02
ACSF2	acyl-CoA synthetase family member 2	HGNC:26101	0.343	3.72E−02
XPNPEP3	X-prolyl aminopeptidase 3	HGNC:28052	0.341	4.48E−03
HTATIP2	HIV−1 Tat interactive protein 2	HGNC:16637	0.339	7.49E−03
HADHB	hydroxyacyl-CoA dehydrogenase trifunctional multienzyme complex subunit beta	HGNC:4803	0.335	8.35E−09
ACAT1	acetyl-CoA acetyltransferase 1	HGNC:93	0.333	7.25E−04
AK3	adenylate kinase 3	HGNC:17376	0.331	1.21E−04
QRSL1	glutaminyl-tRNA amidotransferase subunit QRSL1	HGNC:21020	0.330	1.59E−02
MTO1	mitochondrial tRNA translation optimization 1	HGNC:19261	0.325	4.04E−03
NDUFS4	NADH:ubiquinone oxidoreductase subunit S4	HGNC:7711	0.324	1.89E−04
SERAC1	serine active site containing 1	HGNC:21061	0.324	1.70E−02
ECHDC1	ethylmalonyl-CoA decarboxylase 1	HGNC:21489	0.324	1.95E−04
MTPAP	mitochondrial poly(A) polymerase	HGNC:25532	0.319	1.71E−02
MRPS10	mitochondrial ribosomal protein S10	HGNC:14502	0.318	1.91E−03
RDH14	retinol dehydrogenase 14	HGNC:19979	0.312	1.91E−02
COQ5	coenzyme Q5, methyltransferase	HGNC:28722	0.309	1.68E−03
STOM	stomatin	HGNC:3383	0.308	2.16E−02
GSR	glutathione-disulfide reductase	HGNC:4623	0.304	9.26E−03
LDHB	lactate dehydrogenase B	HGNC:6541	0.298	6.49E−06
UQCRB	ubiquinol-cytochrome c reductase binding protein	HGNC:12582	0.297	5.63E−05
ISCU	iron-sulfur cluster assembly enzyme	HGNC:29882	0.294	4.71E−03
ACOT13	acyl-CoA thioesterase 13	HGNC:20999	0.290	4.20E−02

(*continued on next page*)

Table 3 (*continued*)

TGF-β+RPV8 vs TGF-β UPREGULATED				
hgnc_symbol	**Description**	**HGNC Symbol. Acc.**	**log2FC**	**adjusted p**
COX7A2L	cytochrome c oxidase subunit 7A2 like	HGNC:2289	0.289	6.63E−04
HINT1	histidine triad nucleotide binding protein 1	HGNC:4912	0.288	1.76E−03
TMEM126A	transmembrane protein 126A	HGNC:25382	0.286	3.39E−02
METTL8	methyltransferase 8, methylcytidine	HGNC:25856	0.281	3.15E−02
TFB1M	transcription factor B1, mitochondrial	HGNC:17037	0.280	3.11E−02
MRPS22	mitochondrial ribosomal protein S22	HGNC:14508	0.279	1.43E−03
MTIF3	mitochondrial translational initiation factor 3	HGNC:29788	0.278	2.92E−02
NDUFA12	NADH:ubiquinone oxidoreductase subunit A12	HGNC:23987	0.276	1.05E−02
PLPBP	pyridoxal phosphate binding protein	HGNC:9457	0.275	4.27E−02
SUCLG2	succinate-CoA ligase GDP-forming subunit beta	HGNC:11450	0.270	1.03E−02
LACTB	lactamase beta	HGNC:16468	0.269	2.51E−03
MRPL45	mitochondrial ribosomal protein L45	HGNC:16651	0.265	3.87E−03
NRDC	nardilysin convertase	HGNC:7995	0.264	5.92E−06
ALDH9A1	aldehyde dehydrogenase 9 family member A1	HGNC:412	0.264	1.44E−02
DNAJC15	DnaJ heat shock protein family (Hsp40) member C15	HGNC:20325	0.257	1.64E−02
MCUR1	mitochondrial calcium uniporter regulator 1	HGNC:21097	0.253	4.63E−02
MRPL35	mitochondrial ribosomal protein L35	HGNC:14489	0.250	4.89E−02
GLOD4	glyoxalase domain containing 4	HGNC:14111	0.248	9.19E−03
ALAS1	5'-aminolevulinate synthase 1	HGNC:396	0.247	3.04E−02
TK2	thymidine kinase 2	HGNC:11831	0.241	4.48E−02
MRPL44	mitochondrial ribosomal protein L44	HGNC:16650	0.241	3.31E−02
GHITM	growth hormone inducible transmembrane protein	HGNC:17281	0.241	1.80E−04
MRPL13	mitochondrial ribosomal protein L13	HGNC:14278	0.238	3.06E−02
TOMM20	translocase of outer mitochondrial membrane 20	HGNC:20947	0.233	9.23E−03
MGST3	microsomal glutathione S-transferase 3	HGNC:7064	0.229	2.07E−02
NIT2	nitrilase family member 2	HGNC:29878	0.224	8.09E−03
ATP5PD	ATP synthase peripheral stalk subunit d	HGNC:845	0.214	5.34E−03
UQCRC2	ubiquinol-cytochrome c reductase core protein 2	HGNC:12586	0.212	6.04E−04
MRPS16	mitochondrial ribosomal protein S16	HGNC:14048	0.210	1.74E−02
PARL	presenilin associated rhomboid like	HGNC:18253	0.207	3.05E−02
GARS1	glycyl-tRNA synthetase 1	HGNC:4162	0.199	3.03E−02
DECR1	2,4-dienoyl-CoA reductase 1	HGNC:2753	0.198	2.31E−02
CLPX	caseinolytic mitochondrial matrix peptidase chaperone subunit X	HGNC:2088	0.196	1.80E−02
HADHA	hydroxyacyl-CoA dehydrogenase trifunctional multienzyme complex subunit alpha	HGNC:4801	0.192	8.37E−04
MCL1	MCL1 apoptosis regulator, BCL2 family member	HGNC:6943	0.175	6.74E−03
IARS2	isoleucyl-tRNA synthetase 2, mitochondrial	HGNC:29685	0.175	3.65E−02
TMEM14C	transmembrane protein 14 C	HGNC:20952	0.160	1.69E−02
YME1L1	YME1 like 1 ATPase	HGNC:12843	0.158	3.48E−02
MFF	mitochondrial fission factor	HGNC:24858	0.150	4.73E−02

TGF-β+RPV8 vs TGF-β DOWNREGULATED				
hgnc_symbol	**Description**	**HGNC Symbol. Acc.**	**log2FC**	**adjusted p**
FKBP10	FKBP prolyl isomerase 10	HGNC:18169	−0.957	2.97E−15
GCAT	glycine C-acetyltransferase	HGNC:4188	−0.886	2.40E−07
CRY1	cryptochrome circadian regulator 1	HGNC:2384	−0.802	4.24E−12
SFXN2	sideroflexin 2	HGNC:16086	−0.751	2.63E−03
ALDH1B1	aldehyde dehydrogenase 1 family member B1	HGNC:407	−0.715	3.16E−03
RECQL4	RecQ like helicase 4	HGNC:9949	−0.679	7.65E−04
NT5DC2	5'-nucleotidase domain containing 2	HGNC:25717	−0.655	8.79E−05
ENDOG	endonuclease G	HGNC:3346	−0.609	4.30E−02
MTHFS	methenyltetrahydrofolate synthetase	HGNC:7437	−0.563	4.05E−02
SLC25A42	solute carrier family 25 member 42	HGNC:28380	−0.563	2.11E−03
MPST	mercaptopyruvate sulfurtransferase	HGNC:7223	−0.545	2.41E−05
TST	thiosulfate sulfurtransferase	HGNC:12388	−0.529	1.46E−03
ISOC2	isochorismatase domain containing 2	HGNC:26278	−0.521	1.13E−04
NTHL1	nth like DNA glycosylase 1	HGNC:8028	−0.518	8.29E−03
IDH2	isocitrate dehydrogenase (NADP(+)) 2	HGNC:5383	−0.512	1.59E−04
PXMP2	peroxisomal membrane protein 2	HGNC:9716	−0.506	1.39E−02
PXMP4	peroxisomal membrane protein 4	HGNC:15920	−0.491	2.80E−02
CASP9	caspase 9	HGNC:1511	−0.474	1.71E−03
SLC25A4	solute carrier family 25 member 4	HGNC:10990	−0.471	2.14E−03
ROMO1	reactive oxygen species modulator 1	HGNC:16185	−0.466	1.76E−03
ETFB	electron transfer flavoprotein subunit beta	HGNC:3482	−0.459	1.61E−03
PYCR1	pyrroline−5-carboxylate reductase 1	HGNC:9721	−0.458	3.33E−03
ALDH18A1	aldehyde dehydrogenase 18 family member A1	HGNC:9722	−0.454	8.34E−04
MPV17L2	MPV17 mitochondrial inner membrane protein like 2	HGNC:28177	−0.438	1.28E−03
CLPP	caseinolytic mitochondrial matrix peptidase proteolytic subunit	HGNC:2084	−0.428	3.77E−03
ACP6	acid phosphatase 6, lysophosphatidic	HGNC:29609	−0.421	3.19E−02
DTYMK	deoxythymidylate kinase	HGNC:3061	−0.412	4.51E−03
PUSL1	pseudouridine synthase like 1	HGNC:26914	−0.402	3.76E−03
ALKBH7	alkB homolog 7	HGNC:21306	−0.398	3.65E−02
PICK1	protein interacting with PRKCA 1	HGNC:9394	−0.396	2.34E−03
HDHD5	haloacid dehalogenase like hydrolase domain containing 5	HGNC:1843	−0.395	5.66E−03

(*continued on next page*)

Table 3 (*continued*)

TGF-β+RPV8 vs TGF-β DOWNREGULATED				
hgnc_symbol	**Description**	**HGNC Symbol. Acc.**	**log2FC**	**adjusted p**
MPC1	mitochondrial pyruvate carrier 1	HGNC:21606	−0.385	1.37E−02
PPOX	protoporphyrinogen oxidase	HGNC:9280	−0.383	9.96E−03
FOXRED1	FAD dependent oxidoreductase domain containing 1	HGNC:26927	−0.383	3.28E−03
NLRX1	NLR family member X1	HGNC:29890	−0.373	1.68E−02
GFER	growth factor, augmenter of liver regeneration	HGNC:4236	−0.367	1.10E−02
SLC25A22	solute carrier family 25 member 22	HGNC:19954	−0.364	1.23E−02
MIGA2	mitoguardin 2	HGNC:23621	−0.359	6.17E−03
TOMM40	translocase of outer mitochondrial membrane 40	HGNC:18001	−0.352	1.21E−03
ATP5F1D	ATP synthase F1 subunit delta	HGNC:837	−0.348	1.49E−02
GPAT2	glycerol−3-phosphate acyltransferase 2, mitochondrial	HGNC:27168	−0.346	4.41E−02
SELENOO	selenoprotein O	HGNC:30395	−0.344	1.53E−02
MRPL28	mitochondrial ribosomal protein L28	HGNC:14484	−0.344	1.10E−03
TIMM13	translocase of inner mitochondrial membrane 13	HGNC:11816	−0.342	4.48E−03
ATAD3A	ATPase family AAA domain containing 3A	HGNC:25567	−0.339	1.05E−02
GCDH	glutaryl-CoA dehydrogenase	HGNC:4189	−0.337	3.41E−02
SPHK2	sphingosine kinase 2	HGNC:18859	−0.336	3.38E−03
LETM1	leucine zipper and EF-hand containing transmembrane protein 1	HGNC:6556	−0.335	8.47E−06
DMPK	DM1 protein kinase	HGNC:2933	−0.333	4.10E−02
FASTK	Fas activated serine/threonine kinase	HGNC:24676	−0.327	1.19E−04
MRPS12	mitochondrial ribosomal protein S12	HGNC:10380	−0.323	6.38E−03
NDUFB7	NADH:ubiquinone oxidoreductase subunit B7	HGNC:7702	−0.307	1.78E−02
MRPL4	mitochondrial ribosomal protein L4	HGNC:14276	−0.307	1.28E−03
CYB5R3	cytochrome b5 reductase 3	HGNC:2873	−0.301	3.83E−03
ABCB8	ATP binding cassette subfamily B member 8	HGNC:49	−0.297	1.10E−03
PRKACA	protein kinase cAMP-activated catalytic subunit alpha	HGNC:9380	−0.295	8.62E−03
MCCC2	methylcrotonyl-CoA carboxylase subunit 2	HGNC:6937	−0.287	1.39E−02
FIS1	fission, mitochondrial 1	HGNC:21689	−0.287	4.23E−02
NDUFA11	NADH:ubiquinone oxidoreductase subunit A11	HGNC:20371	−0.283	1.44E−02
ACOT7	acyl-CoA thioesterase 7	HGNC:24157	−0.279	2.72E−02
BCAT2	branched chain amino acid transaminase 2	HGNC:977	−0.279	4.06E−02
TSPO	translocator protein	HGNC:1158	−0.270	4.44E−02
BCKDK	branched chain keto acid dehydrogenase kinase	HGNC:16902	−0.265	3.89E−02
PRDX2	peroxiredoxin 2	HGNC:9353	−0.261	1.22E−02
MYO19	myosin XIX	HGNC:26234	−0.261	4.98E−03
HAGH	hydroxyacylglutathione hydrolase	HGNC:4805	−0.253	4.29E−02
AURKAIP1	aurora kinase A interacting protein 1	HGNC:24114	−0.250	1.98E−02
CHCHD2	coiled-coil-helix-coiled-coil-helix domain containing 2	HGNC:21645	−0.248	2.80E−02
RNASEH1	ribonuclease H1	HGNC:18466	−0.245	3.65E−02
MRPL18	mitochondrial ribosomal protein L18	HGNC:14477	−0.241	1.86E−02
PITRM1	pitrilysin metallopeptidase 1	HGNC:17663	−0.241	5.63E−05
RCC1L	RCC1 like	HGNC:14948	−0.240	1.41E−02
DHX30	DExH-box helicase 30	HGNC:16716	−0.233	8.57E−04
MSRB3	methionine sulfoxide reductase B3	HGNC:27375	−0.220	1.14E−02
POLRMT	RNA polymerase mitochondrial	HGNC:9200	−0.217	2.73E−02
RHOT2	ras homolog family member T2	HGNC:21169	−0.207	4.61E−02

metabolic activities including glycolysis and glutaminolysis. Of note, there is evidence that different antifibrogenic compounds diminish both OCR and ECAR in aHSCs [13], which is in line with our findings regarding the capacity of RPV to reverse the stimulating effect of TGF-β on these bioenergetics' parameters. $\Delta\psi_m$ is also altered during HSC activation, though published data related with this are controversial. There is evidence of an increase in $\Delta\psi_m$ in the case of LX2 cells and rat HSCs when cultured on regular tissue culture plasticware (referred to as an activated or fibrogenic phenotype) compared to less-active (non--fibrogenic) HSCs generated by culture on the matrigel Geltrex [11] or the rat HSC cell line HSC-T6 when exposed to PDGF-BB for 24 h [30]. In clear contrast, both LX2 and primary HSCs exposed to profibrogenic fine particulate matter (PM2.5) were reported to display lower $\Delta\psi_m$ [31]. Some studies have demonstrated that *in vitro* antifibrogenic treatments with natural compounds diminish $\Delta\psi_{m,}$ such as in the case of spontaneously activated HSC-T6 cells under short-term exposure (up to 60 min) to saikosaponin [13], or PDFG-BB-activated HSC-T6 cells co-treated with dydimin (24 h) [30]. However, in our experiments, RPV (48 h) seemed to reverse the drop in $\Delta\psi_m$ triggered by TGF-β in LX2. The root of these discrepancies is yet to be determined and awaits further research.

The role of physiological uncoupling of respiration from OXPHOS in specific energetic scenarios such as HSC activation is not fully clear. Herein, we report that the respiratory rate in TGF-β-treated cells increases while the proton leak is enhanced, which indicates either an increase in the IMM proton permeability due to a change in the membrane proton conductance, or a decrease in the efficiency of the proton pumps, which means higher levels of electron transfer are needed for the same number of protons be pumped out, known as redox slipping. Of note, apart from heat dissipation and prevention of oxidative stress, other suggested roles of physiological uncoupling include increased TCA cycle flux in support of metabolite synthesis and exchange, as TCA cycle intermediates provide carbon backbones for non-essential amino acids and other anabolic reactions through cataplerosis. This is related to the fact that the transport of certain molecules into mitochondria depends on compensated proton symport (electroneutral protonated acids), and is thus dependent on the pH gradient component of $\Delta\Psi_m$. One such molecule is pyruvate, the end-product of glycolysis, a major substrate of oxidative metabolism, and a hub molecule for the synthesis of glucose, lactate, fatty acids and amino acids. Mitochondrial import of pyruvate requires VDAC to cross the OMM in a passive fashion and also depends on the mitochondrial pyruvate carrier (MPC) to shuttle pyruvate though the IMM. This latter process is dependent upon the proton gradient and is stimulated by an increase in matrix pH [32]. MPC is composed of two proteins, MPC1 and MPC2, which form a hetero-oligomeric complex. Interestingly, we show in this study that RPV treatment leads to a

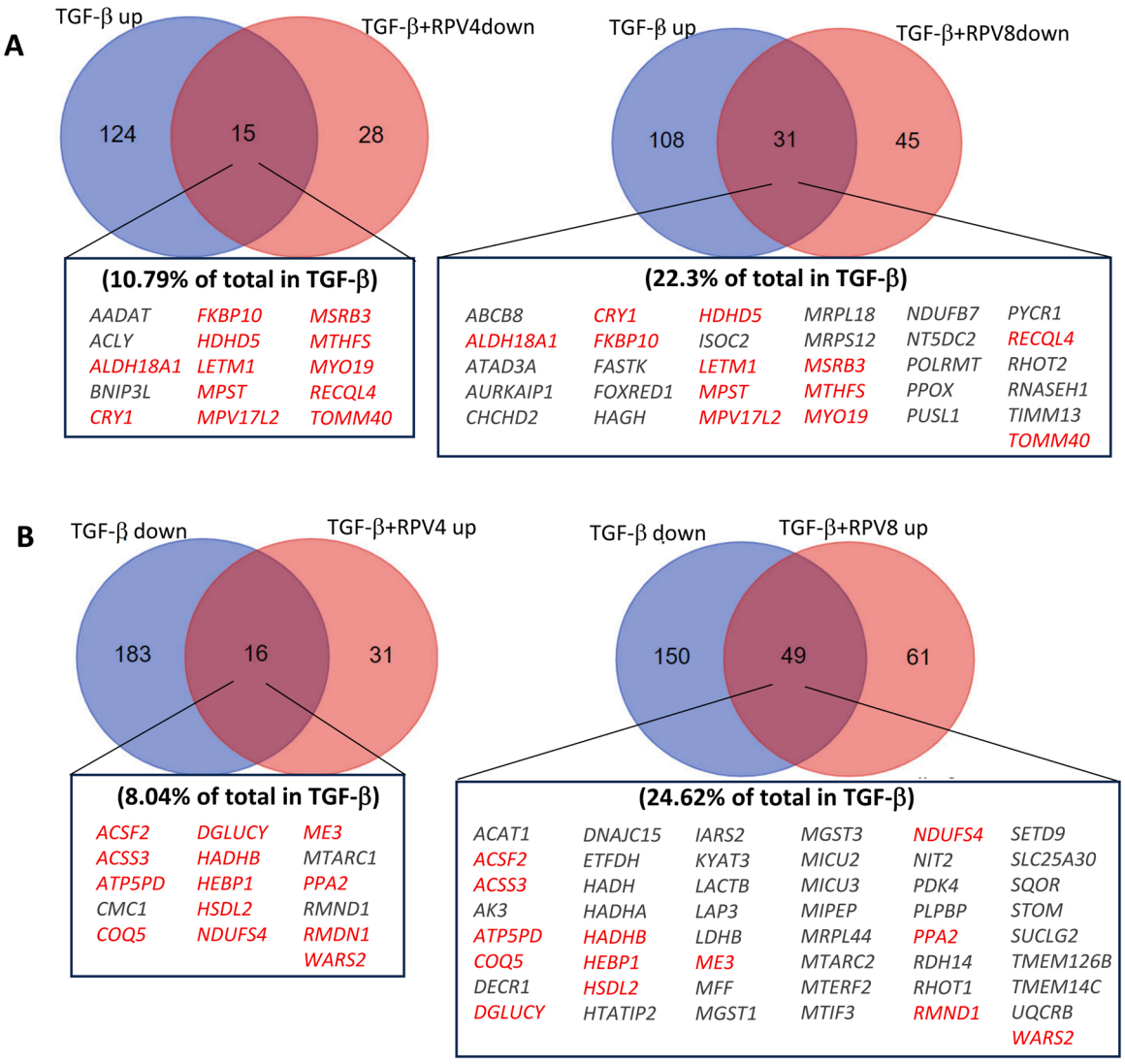

Fig. 7. RNA sequencing analysis of differentially expressed genes encoding mitochondrial proteins mito-DEGs (II). Primary human HSC were treated with Vehicle (Veh), TGF-β alone or in presence of RPV (4 or 8 μM) (n=6). Venn diagrams showing significantly upregulated (A) or significantly downregulated (B) mito-DEGs in cells exposed to TGF-β vs Veh and the genes whose expression was reversed by the co-treatment TGF-β+RPV4 or TGF-β+RPV8 (listed in an alphabetical order in the boxes). The names of the mito-DEGs common for TGF-β+RPV4 and TGF-β+RPV8 are shown in red.

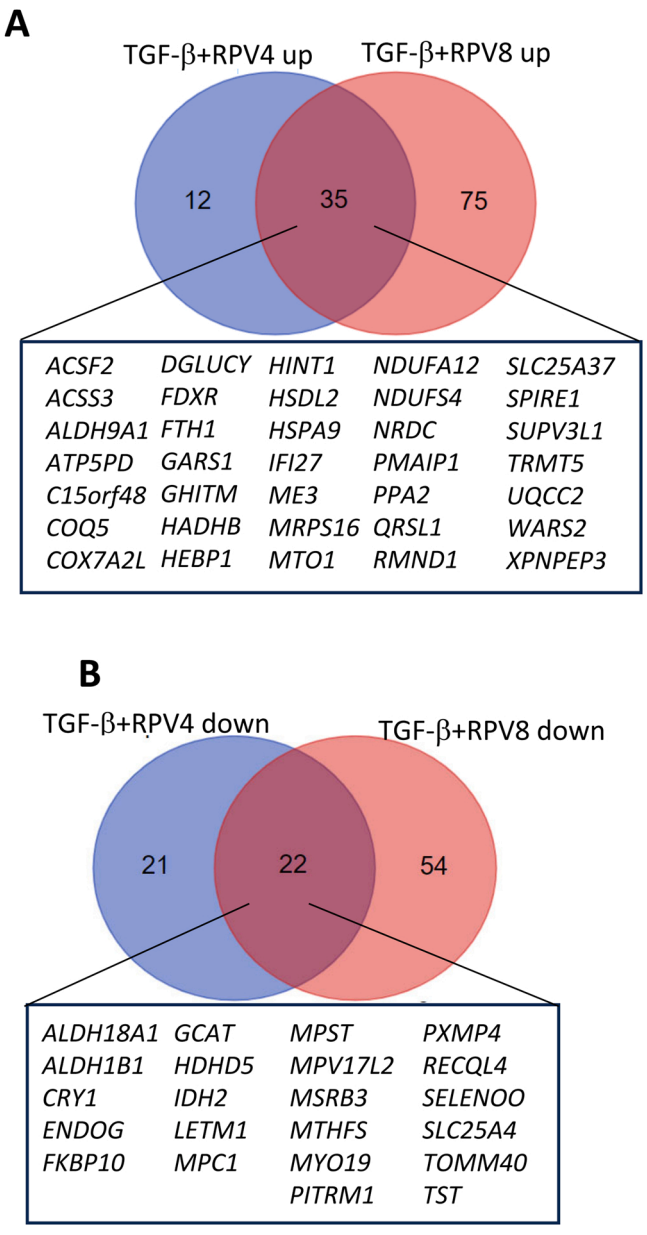

Fig. 8. RNA sequencing analysis of differentially expressed genes encoding mitochondrial proteins (mito-DEGs) (III). Primary human HSCs were treated with Vehicle, TGF-β alone or in presence of RPV (4 or 8 μM) (n=6). Venn diagrams showing significantly upregulated (A) or significantly downregulated (B) mito-DEGs in cells exposed to the co-treatment TGF-β+RPV4 or TGF-β+RPV8, independently of whether they were reversed or not with respect to TGF-β. The names of the mito-DEGs common for TGF-β+RPV4 and TGF-β+RPV8 treatments are listed in alphabetical order in the boxes.

decrease in the mRNA expression of MPC1 in primary human HSCs exposed to TFG-β. This finding is relevant given the fact that MPC inhibition in HSCs produces antifibrotic effects in murine models of MASH [33,34], and MPC function has also been proven to be a pillar of fibrosis in other organs; for example, for the maintenance of the corneal myofibroblast phenotype *in vitro* and *in vivo* [35]. In light of this, MPC may constitute a promising antifibrotic target.

To date, it is still not clear whether enhanced ATP production in aHSC is due to increased mitochondrial number (biogenesis) or enhanced functioning of existing mitochondria, or both. Apart from reprogramming the functions of existing mitochondria, the increased energy required for HSCs to become activated is thought to be achieved by increased mitochondrial biogenesis and the significantly increased expression of genes associated with it in aHSCs versus qHSCs [8]. In the present study, TGF-β-activated LX2 cells displayed enhanced mitochondrial mass, an effect that was absent when there was co-treatment with RPV. In addition, TGF-β increased the content of key mitochondrial proteins in a specific manner, an effect that was prevented by co-treatment with RPV. This occurs with mtDNA-encoded ND1, a protein necessary for complex I assembly and stability, whose abundance is crucial for mitochondrial respiration [36].

Several studies have addressed the alterations that occur in mitochondrial dynamics during HSC activation, including the effect of TGF-β and that of antifibrogenic compounds. For instance, treatment of TGF-β-exposed LX2 cells with *Turnera diffusa* extract led to a decrease in the protein levels of MFN2, although the authors did not provide further evidence of the functional alteration of mitochondrial fusion/fission in their model [37]. In our study, exposure of LX2 to TGF-β led to increased mitochondrial fission, which was ameliorated in the presence of RPV. In addition, it has been suggested that spontaneously activated primary rat HSCs under fluorescence microscopy display fused mitochondria on day 7 while showing diminished MFN1 and 2 levels [7]. The same study also provided evidence of increased levels of MFN1 and 2 on day 1 of HSC activation. These discrepancies clearly underline the complex nature of the modification of mitochondrial dynamics during HSC activation and highlight the need for it to be interpreted with great caution. Our study also shows that the mitochondria in activated LX2 cells (exposed to TGF-β) are altered in size and shape, as revealed by fluorescence microscopy and TEM imaging. This is in line with other reports of mitochondria in activated HSC being smaller and more rounded (less elongated) than in quiescent cells, such as in the case of succinate-induced activation of LX2 [16] or TGF-β-activated HSC-T6 cells [38], and endorses that antifibrotic treatments can prevent this change.

Our study of the antifibrogenic action of RPV reveals various potential targets. Following the criteria of statistical potency (lower *p* value) and/or higher fold change, several mitoDEGs stand out. FK506-binding protein 10 (*FKBP10*) and mitochondria-associated myosin 19 (*MYO19*) are both upregulated in cells exposed to TGF-β, while this increase is reversed upon co-treatment with RPV4 or RPV8. According to the MitoCarta Dataset, FKBP10 (also termed FKBP65) is present in the IMS and has a shared domain (mitochondrial and non-mitochondrial). The ER-resident FKBP10 is associated with collagen synthesis, a complex process in which three chains of pro-collagen - two of pro-α1 and one of pro-α2 - are folded into a triple helix in a zipper-like fashion. This process involves multiple folding catalysts, including peptidyl-proline isomerases (PPIases) such as FKBP10, FKBP11, and FKBP14, which are considered to be rate-limiting enzymes, as the number of proline residues in collagen molecule is relatively high [39]. *MYO19*, which according to MitoCarta Dataset is located in the MOM and has a shared domain (mitochondrial and non-mitochondrial), transports mitochondria on actin tracks in living cells. While not much is known of this protein in the liver, it has appeared in a meta-analysis as part of a human hepatic gene expression signature of non-alcoholic fatty liver disease progression [40].

In conclusion, here we provide evidence that RPV interferes with mitochondrial function in HSCs activated by TGF-β, which is of relevance in understanding the mechanisms responsible for the antifibrotic and hepatoprotective actions of this drug already demonstrated *in vitro* and *in vivo*. Our results confirm mitochondria as a promising target in the search of novel therapies aimed at managing CLDs, and particularly LF.

Funding

This research was funded by the Instituto de Salud Carlos III (PI22-00424, CIBER CB06/04/0071 -co-funded by the European Regional Development Fund of the European Union-), Generalitat Valenciana

Table 4
Analysis of the Mitopathways hierarchy in the differentially expressed genes encoding mitochondrial proteins (mito-DEGs) using RNA sequencing data of TGF-β+RPV8 or TGF-β+RPV4 vs TGF-β-activated-HSCs. The mito-DEGs analyzed are those common for TGF-β+RPV4 and TGF-β+RPV8 whose expression was reversed compared to the treatment with TGF-β only. Primary human HSCs were treated with TGF-β alone or in the presence of 4 μM RPV or 8 μM RPV for 48 h (n=6), adjusted p or $p<0.05$. The tables show Mitopathways of the Mito-DEGs that were significantly upregulated (A) or downregulated (B) in TGF-β-exposed cells and whose expression was reversed in cells exposed to TGF-β+RPV4 or TGF-β+RPV8.

A

MitoPathway	MitoPathways Hierarchy
Mitochondrial central dogma	Mitochondrial central dogma > Translation > Mitochondrial ribosome assembly > mtDNA maintenance > mtDNA repair
Metabolism	Metabolism > Vitamin metabolism > Folate and 1-C metabolism > Amino acid metabolism > Proline metabolism > Sulfur metabolism > Detoxification > Xenobiotic metabolism > ROS and glutathione metabolism
Protein import, sorting and homeostasis	Protein import, sorting and homeostasis > Protein homeostasis > Chaperones > TOM
Signaling	Signaling > Calcium homeostasis > Calcium cycle
Mitochondrial dynamics and surveillance	Mitochondrial dynamics and surveillance > Trafficking

B

MitoPathway	MitoPathways Hierarchy
Mitochondrial central dogma	Mitochondrial central dogma > mtRNA metabolism > mtRNA metabolism > mtRNA granules > Translation > mt-tRNA synthetases > mtDNA maintenance
Metabolism	Metabolism > Nucleotide metabolism > Nucleotide synthesis and processing > Lipid metabolism > Fatty acid oxidation > Amino acid metabolism > Lysine metabolism > Carbohydrate metabolism > TCA-associated > Carbohydrate metabolism > Ketone metabolism > Metals and cofactors > Coenzyme Q metabolism
OXPHOS	OXPHOS > Complex I > CI subunits > Complex V > CV subunits

(AICO2021/017 and CIPROM/2021/044), FISABIO (UGP-21-236) and the Spanish Ministry of Science and Innovation MCIN/AEI/10.13039/501100011033, co-funded by the European Regional Development Fund of the European Union - A way to make Europe (PID2021-127945OB-I00). A.M.B. and I.F.M are the recipients of Postgraduate Trainee Research Grants from the Spanish Ministry of Science, Innovation and Universities (FPU19/05064 and FPU18/02435).

CRediT authorship contribution statement

Ana M Benedicto: Methodology, Investigation, Data curation. **Ana Blas-Garcia:** Investigation, Funding acquisition, Conceptualization. **Nadezda Apostolova:** Writing – original draft, Project administration, Funding acquisition, Conceptualization. **Pedro Diaz-Pozo:** Resources, Methodology. **Dimitri Dorcaratto:** Resources. **Federico Lucantoni:** Methodology, Investigation, Conceptualization. **Isabel Fuster-Martinez:** Methodology, Investigation, Data curation. **Juan V Esplugues:** Supervision, Funding acquisition. **Elena Muñoz-Forner:** Resources. **Victor M Victor:** Methodology, Investigation, Data curation.

Declaration of Competing Interest

The authors declare that the research was conducted in the absence of any commercial or financial relationships that could be construed as a potential conflict of interest.

Acknowledgements

The authors thank Brian Normanly (University of Valencia/CIBERehd, Spain) for his editorial assistance, María Ortega Albiach (Genothek Solutions, Valencia, Spain) for helping with the computational analysis and visualization of the RNA-seq data and Mario Soriano Navarro (Centro de Investigación Principe Felipe, Valencia, Spain) for assistance with TEM.

References

[1] L. Campana, J.P. Iredale, Regression of liver fibrosis, Semin. Liver Dis. 37 (1) (2017) 1–10, https://doi.org/10.1055/s-0036-1597816.
[2] R. Bataller, D.A. Brenner, Liver fibrosis, J. Clin. Invest. 115 (2) (2005) 209–218, https://doi.org/10.1172/JCI24282. Erratum in: J. Clin. Invest. 115(4) (2005) 1100.
[3] J.E. Puche, Y. Saiman, S.L. Friedman, Hepatic stellate cells and liver fibrosis, Compr. Physiol. 3 (4) (2013) 1473–1492, https://doi.org/10.1002/cphy.c120035.
[4] T. Tsuchida, S.L. Friedman, Mechanisms of hepatic stellate cell activation, Nat. Rev. Gastroenterol. Hepatol. 14 (7) (2017) 397–411, https://doi.org/10.1038/nrgastro.2017.38.
[5] C. Hellerbrand, B. Stefanovic, F. Giordano, E.R. Burchardt, D.A. Brenner, The role of TGF[beta]1 in initiating hepatic stellate cell activation in vivo, J. Hepatol. 30 (1999) 77–87.
[6] K. Baghaei, S. Mazhari, S. Tokhanbigli, G. Parsamanesh, H. Alavifard, D. Schaafsma, S. Ghavami, Therapeutic potential of targeting regulatory mechanisms of hepatic stellate cell activation in liver fibrosis, Drug Discov. Today 27 (4) (2022) 1044–1061, https://doi.org/10.1016/j.drudis.2021.12.012.
[7] N. Smith-Cortinez, K. van Eunen, J. Heegsma, S.A. Serna-Salas, S. Sydor, L. P. Bechmann, H. Moshage, B.M. Bakker, K.N. Faber, Simultaneous induction of glycolysis and oxidative phosphorylation during activation of hepatic stellate cells reveals novel mitochondrial targets to treat liver fibrosis, Cells 9 (11) (2020) 2456, https://doi.org/10.3390/cells9112456.
[8] D. Ezhilarasan, D, Mitochondria: a critical hub for hepatic stellate cells activation during chronic liver diseases, Hepatobiliary Pancreat. Dis. Int 20 (4) (2021) 315–322, https://doi.org/10.1016/j.hbpd.2021.04.010.
[9] H.W. Lim, H.Y. Lim, K.P. Wong, Uncoupling of oxidative phosphorylation by curcumin: implication of its cellular mechanism of action, Biochem. Biophys. Res. Commun. 389 (1) (2009) 187–192, https://doi.org/10.1016/j.bbrc.2009.08.121.
[10] E.L. Guimarães, J. Best, L. Dollé, M. Najimi, E. Sokal, L.A. van Grunsven, Mitochondrial uncouplers inhibit hepatic stellate cell activation, BMC Gastroenterol. 12 (2012) 68, https://doi.org/10.1186/1471-230X-12-68.
[11] P. Gajendiran, L.I. Vega, K. Itoh, H. Sesaki, M.R. Vakili, A. Lavasanifar, K. Hong, E. Mezey, S. Ganapathy-Kanniappan, Elevated mitochondrial activity distinguishes fibrogenic hepatic stellate cells and sensitizes for selective inhibition by mitotropic

doxorubicin, J. Cell. Mol. Med. 22 (4) (2018) 2210–2219, https://doi.org/10.1111/jcmm.13501.
[12] M. Bae, Y. Lee, Y.K. Park, D.G. Shin, P. Joshi, S.H. Hong, N. Alder, S.I. Koo, Ji-Y. Lee, Astaxanthin attenuates the increase in mitochondrial respiration during the activation of hepatic stellate cells, J. Nutr. Biochem 71 (2019) 82–89, https://doi.org/10.1016/j.jnutbio.2019.06.001.
[13] M.F. Chen, S.J. Huang, C.C. Huang, P.S. Liu, K.I. Lin, C.W. Liu, W.C. Hsieh, L. Y. Shiu, C.H. Chen, Saikosaponin d induces cell death through caspase-3-dependent, caspase-3-independent and mitochondrial pathways in mammalian hepatic stellate cells, BMC Cancer 16 (2016) 532, https://doi.org/10.1186/s12885-016-2599-0.
[14] G. Poli, Pathogenesis of liver fibrosis: role of oxidative stress, Mol. Asp. Med. 21 (3) (2000) 49–98, https://doi.org/10.1016/s0098-2997(00)00004-2.
[15] P. Greenwel, J.-A. Domínguez-Rosales, G. Mavi, A.M. Rivas-Estilla, M. Rojkind, Hydrogen peroxide: a link between acetaldehyde-elicited α1(i) collagen gene up-regulation and oxidative stress in mouse hepatic stellate cells, Hepatology 31 (1) (2000) 109–116, https://doi.org/10.1002/hep.510310118.
[16] G. Nguyen, S.Y. Park, D.V. Do, D.H. Choi, E.H. Cho, Gemigliptin alleviates succinate-induced hepatic stellate cell activation by ameliorating mitochondrial dysfunction, Endocrinol. Metab. 37 (6) (2022) 918–928, https://doi.org/10.3803/EnM.2022.1530.
[17] A. Martí-Rodrigo, F. Alegre, Á.B. Moragrega, F. García-García, P. Martí-Rodrigo, A. Fernández-Iglesias, J. Gracia-Sancho, N. Apostolova, J.V. Esplugues, A. Blas-García, Rilpivirine attenuates liver fibrosis through selective STAT1-mediated apoptosis in hepatic stellate cells, Gut 69 (5) (2020) 920–932, https://doi.org/10.1136/gutjnl-2019-318372.
[18] F. Lucantoni, A.M. Benedicto, A. Gruevska, Á.B. Moragrega, I. Fuster-Martínez, J. V. Esplugues, A. Blas-García, N. Apostolova, Implication of autophagy in the antifibrogenic effect of Rilpivirine: when more is less, Cell Death Dis. 13 (4) (2022) 385, https://doi.org/10.1038/s41419-022-04789-7.
[19] L. Xu, A.Y. Hui, E. Albanis, M.J. Arthur, S.M. O'Byrne, W.S. Blaner, P. Mukherjee, S.L. Friedman, F.J. Eng, Human hepatic stellate cell lines, LX-1 and LX-2: new tools for analysis of hepatic fibrosis, Gut 54 (1) (2005) 142–151, https://doi.org/10.1136/gut.2004.042127.
[20] A. Casini, M. Pinzani, S. Milani, C. Grappone, G. Galli, A.M. Jezequel, D. Schuppan, C.M. Rotella, C. Surrenti, Regulation of extracellular matrix synthesis by transforming growth factor β1 in human fat-storing cells, Gastroenterology 105 (1) (1993) 245–253, https://doi.org/10.1016/0016-5085(93)90033-9.
[21] A.J. Valente, L.A. Maddalena, E.L. Robb, F. Moradi, J.A. Stuart, A simple ImageJ macro tool for analyzing mitochondrial network morphology in mammalian cell culture, Acta Histochem 119 (3) (2017) 315–326, https://doi.org/10.1016/j.acthis.2017.03.001.
[22] J. Lam, P. Katti, M. Biete, M. Mungai, S. AshShareef, K. Neikirk, E. Garza Lopez, Z. Vue, T.A. Christensen, H.K. Beasley, T.A. Rodman, S.A. Murray, J.L. Salisbury, B. Glancy, J. Shao, R.O. Pereira, E.D. Abel, A. Jr, A. Hinton, A universal approach to analyzing transmission electron microscopy with ImageJ, Cells 10 (9) (2021) 2177, https://doi.org/10.3390/cells10092177.
[23] X. Gu, Y. Ma, Y. Liu, Q. Wan, Measurement of mitochondrial respiration in adherent cells by Seahorse XF96 cell mito stress test, STAR Protoc. 2 (1) (2020) 100245, https://doi.org/10.1016/j.xpro.2020.100245.
[24] M. Arbaizar-Rovirosa, J. Pedragosa, J.J. Lozano, C. Casal, A. Pol, M. Gallizioli, A. M. Planas, Aged lipid-laden microglia display impaired responses to stroke, EMBO Mol. Med. 15 (2) (2023) e17175, https://doi.org/10.15252/emmm.202217175.
[25] M.I. Love, W. Huber, S. Anders, Moderated estimation of fold change and dispersion for RNA-seq data with DESeq2, Genome Biol. 15 (12) (2014) 550, https://doi.org/10.1186/s13059-014-0550-8.
[26] S. Rath, R. Sharma, R. Gupta, T. Ast, C. Chan, T.J. Durham, R.P. Goodman, Z. Grabarek, M.E. Haas, W.H.W. Hung, P.R. Joshi, A.A. Jourdain, S.H. Kim, A. V. Kotrys, S.S. Lam, J.G. McCoy, J.D. Meisel, M. Miranda, A. Panda, A. Patgiri, S. Rogers, S. Sadre, H. Shah, O.S. Skinner, T.L. To, M.A. Walker, W. Wang, P. S. Ward, J. Wengrod, C.C. Yuan, S.E. Calvo, V.K. Mootha, MitoCarta3.0: an updated mitochondrial proteome now with sub-organelle localization and pathway annotations, Nucleic Acids Res. 49 (D1) (2021) D1541–D1547, https://doi.org/10.1093/nar/gkaa1011.
[27] J. Chen, J. Cao, P. Wang, X. He, NT5DC2 is a novel prognostic marker in human hepatocellular carcinoma, Oncol. Lett. 20 (4) (2020) 70, https://doi.org/10.3892/ol.2020.11931.
[28] X. Sun, Y. Yang, D. Zhu, H. Qian, Y. Duan, X. He, X. Gu, W. Sun, Y. Zhu, Expression of Septin4 in human hepatic stellate cells LX-2 stimulated by LPS, Inflammation 36 (3) (2013) 539–548, https://doi.org/10.1007/s10753-012-9575-x.
[29] D. Zhu, J. Wang, X. Sun, J. Chen, Y. Duan, J. Pan, T. Xu, Y. Qin, X. He, C. Huang, Septin4_i1 regulates apoptosis in hepatic stellate cells through peroxisome proliferator-activated receptor-γ/Akt/B-cell lymphoma 2 pathway, J. Histochem. Cytochem 63 (3) (2015) 163–169, https://doi.org/10.1369/0022155414567230.
[30] X. Lin, F. Bai, J. Nie, S. Lu, C. Lu, X. Zhu, J. Wei, Z. Lu, Q. Huang, didymin alleviates hepatic fibrosis through inhibiting ERK and PI3K/Akt pathways via regulation of Raf kinase inhibitor protein, Cell Physiol. Biochem 40 (6) (2016) 1422–1432, https://doi.org/10.1159/000453194.
[31] Y.N. Qiu, G.H. Wang, F. Zhou, J.J. Hao, L. Tian, L.F. Guan, X.K. Geng, Y.C. Ding, H. W. Wu, K.Z. Zhang, PM2.5 induces liver fibrosis via triggering ROS-mediated mitophagy, Ecotoxicol. Environ. Saf. 167 (2019) 178–187, https://doi.org/10.1016/j.ecoenv.2018.08.050.
[32] C.N. Cunningham, J. Rutter, 20,000 picometers under the OMM: diving into the vastness of mitochondrial metabolite transport, EMBO Rep. 21 (5) (2020) e50071, https://doi.org/10.15252/embr.202050071.
[33] K.S. McCommis, W.T. Hodges, E.M. Brunt, I. Nalbantoglu, W.G. McDonald, C. Holley, H. Fujiwara, J.E. Schaffer, J.R. Colca, B.N. Finck, Targeting the mitochondrial pyruvate carrier attenuates fibrosis in a mouse model of nonalcoholic steatohepatitis, Hepatology 65 (5) (2017) 1543–1556, https://doi.org/10.1002/hep.29025.
[34] M. Habibi, D. Ferguson, S.J. Eichler, M.M. Chan, A. LaPoint, T.M. Shew, M. He, A.J. Lutkewitte, J.D. Schilling, K.Y. Cho, G.J. Patti, B.N. Finck, Mitochondrial pyruvate carrier inhibition attenuates hepatic stellate cell activation and liver injury in a mouse model of metabolic dysfunction-associated steatotic liver disease, BioRxiv 2023.02.13.528384. ⟨doi:10.1101/2023.02.13.528384⟩.
[35] K.I. Jeon, A. Kumar, C.L. Callan, M. DeMagistris, S. MacRae, K. Nehrke, K. R. Huxlin, Blocking mitochondrial pyruvate transport alters corneal myofibroblast phenotype: a new target for treating fibrosis, Invest. Ophthalmol. Vis. Sci. 64 (13) (2023) 36, https://doi.org/10.1167/iovs.64.13.36.
[36] L. Iommarini, A. Ghelli, C.V. Tropeano, I. Kurelac, G. Leone, S. Vidoni, A. Lombes, M. Zeviani, G. Gasparre, A.M. Porcelli, Unravelling the effects of the mutation m.3571insC/MT-ND1 on respiratory complexes structural organization, Int. J. Mol. Sci. 19 (2018) 764, https://doi.org/10.3390/ijms1903076.
[37] D.R. Rodríguez-Rodríguez, S.A. Lozano-Sepulveda, C. Delgado-Montemayor, N. Waksman, P. Cordero-Perez, A.M. Rivas-Estilla, Turnera diffusa extract attenuates profibrotic, extracellular matrix and mitochondrial markers in activated human hepatic stellate cells (HSC), Ann. Hepatol. 22 (2021) 100281, https://doi.org/10.1016/j.aohep.2020.10.009.
[38] X. Peng, H. Yang, L. Tao, J. Xiao, Y. Zeng, Y. Shen, X. Yu, F. Zhu, J. Qin, Fluorofenidone alleviates liver fibrosis by inhibiting hepatic stellate cell autophagy via the TGF-β1/Smad pathway: implications for liver cancer, Peer J. 11 (2023) e16060, https://doi.org/10.7717/peerj.16060.
[39] T. Luangmonkong, W. Parichatikanond, P. Olinga, Targeting collagen homeostasis for the treatment of liver fibrosis: opportunities and challenges, Biochem. Pharm. 215 (2023) 115740, https://doi.org/10.1016/j.bcp.2023.115740.
[40] M. Ryaboshapkina, M. Hammar, Human hepatic gene expression signature of non-alcoholic fatty liver disease progression, a meta-analysis, Sci. Rep. 7 (1) (2017) 12361, https://doi.org/10.1038/s41598-017-10930-w.